# A unified evolutionary origin for the ubiquitous protein transporters SecY and YidC

Aaron J. O. Lewis and Ramanujan S. Hegde

MRC Laboratory of Molecular Biology
Francis Crick Avenue, Cambridge, CB2 0QH, UK

Correspondence: aaron.ohare.lewis@gmail.com or rhegde@mrc-lmb.cam.ac.uk

## Abstract

Cells use transporters to move protein across membranes, but the origins of the most ancient transporters are unknown. Here, we analyse the protein-conducting channel SecY. Features conserved by its two duplicated halves suggest that their common ancestor was an antiparallel homodimeric channel. Structural searches with individual halves detect exceptional similarity with the YidC family of membrane protein transporters. Their shared fold comprises a three-helix bundle interrupted by a helical hairpin. In YidC this hairpin is cytosolic and facilitates substrate delivery, whereas in SecY it forms the substrate-binding transmembrane helices of the lateral gate. In both, the three-helix bundle forms a hydrophilic groove for translocation, delimited by a conserved hydrophobic residue. We propose that SecY originated as a homodimeric YidC homolog. Many YidC homologs now use this interface to heterodimerise with a conserved partner. Unification of the two ubiquitous protein transporter families reconstructs a key step in the evolution of cells.

## Introduction

By the time of the last universal common ancestor (cenancestor), cells had already evolved a hydrophobic membrane and integral membrane proteins (IMPs) which carried out core metabolic functions (Coleman et al., 2021; Williams et al., 2017). Among those IMPs was SecY, a protein-conducting channel (Park and Rapoport, 2012). As is typical for channels, SecY (termed Sec61 in eukaryotes) catalyses the translocation of hydrophilic substrates across the hydrophobic membrane by creating a conducive hydrophilic environment inside the membrane. The substrates which it translocates are secretory proteins and the extracytoplasmic segments of IMPs.

SecY typically requires that its hydrophilic translocation substrates be connected to a hydrophobic α-helix (von Heijne, 1985; Krogh et al., 2001; Petersen et al., 2011). These hydrophobic helices serve as signals which open the SecY channel (Jungnickel and Rapoport, 1995; Li et al., 2016; Voorhees and Hegde, 2016). SecY is comprised of two separate halves (Van den Berg et al., 2004) which open like a clamshell when a helix binds to the lipid interface between them (Figure 1a). Spreading the halves apart destabilises a plug which sits between them, opening a hydrophilic pore that spans the width of the membrane. By binding at this site, the signal also threads one of its hydrophilic flanking regions through the hydrophilic pore, thereby initiating its translocation.

A set of conserved hydrophobic residues that line the narrowest part of the translocation pore form a gasket-like seal around the translocating chain (Ma et al., 2019). These residues, which are contributed by both halves of SecY, are known collectively as the pore ring. They not only maintain the ion permeability barrier across the membrane (Dalal and Duong, 2009; Park and Rapoport, 2011), but also bind the plug when the channel is closed (Van den Berg et al., 2004).

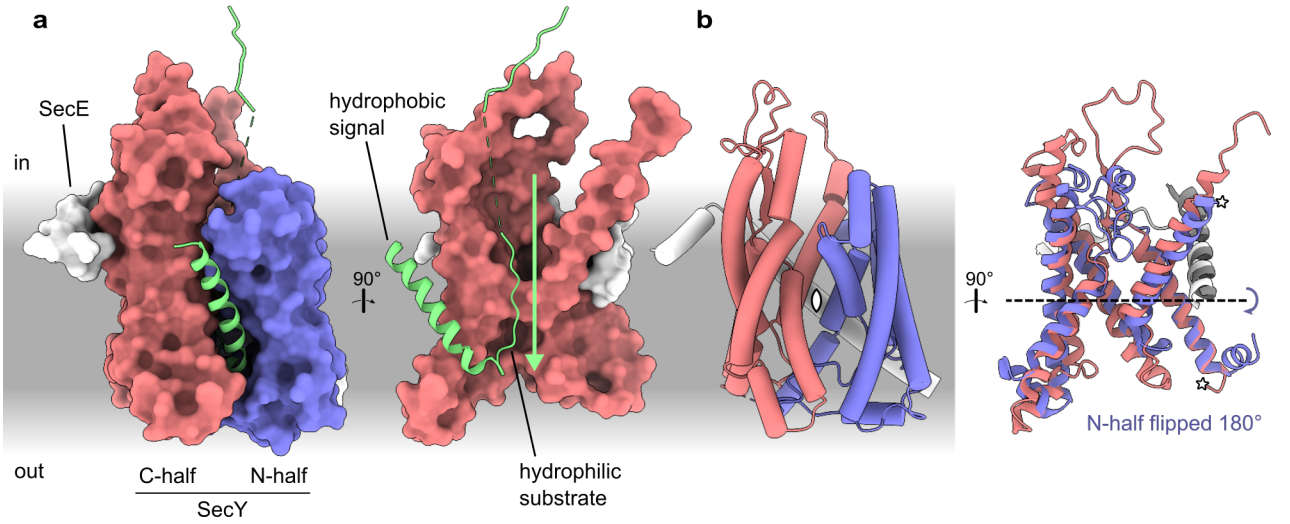


**Figure 1.** Structure and pseudosymmetry of the SecY protein channel. **a** Left: Structure of the channel engaged by a secretory substrate: *Geobacillus thermodenitrificans* SecYE engaged by proOmpA (Protein Data Bank ID [PDB] 6itc). The cytosolic ATPase SecA is present in the model but not shown. Right: Rotated view of only the SecY N-half and substrate. **b** Pseudosymmetry of the N- and C-halves. Left: SecYE shown as tubes with the pseudo-$C_2$ symmetry axis denoted by a pointed oval. Right: Rotated view in ribbon representation. The N-half has been rotated 180° around the pseudo-$C_2$ symmetry axis and aligned to the C-half. SecE is divided where it intersects the symmetry axis into N-terminal (white) and C-terminal (grey) segments. A dashed black line indicates the same pseudo-$C_2$ symmetry axis shown at left after a 90° rotation. Stars indicate where the halves were split.

The site between SecY's halves where signals bind is called the lateral gate. After binding and initiating translocation, sufficiently hydrophobic signals can diffuse away from the lateral gate into the surrounding hydrophobic membrane. Many signals, particularly those at the N-terminus of secretory proteins, are ultimately cleaved off by signal peptidase, a membrane-anchored protease whose active site resides on the extracytoplasmic side of the membrane (Paetzel et al., 2002). Longer and more hydrophobic signals that are not cleaved serve as the transmembrane helices (TMHs) of IMPs (White and von Heijne, 2005).

SecY is the only ubiquitous transporter for protein secretion. There is however a second ubiquitous superfamily of protein transporters which is specialised for IMP integration, Oxa1 (Anghel et al., 2017). The Oxa1 superfamily consists of four member families, each of which now has a known atomic structure. One, YidC, is found in the prokaryotic plasma membrane (Borowska et al., 2015; Kumazaki et al., 2014), whereas the other three are paralogs located in the eukaryotic endoplasmic reticulum (ER): TMCO1 (McGilvray et al., 2020), EMC3 (Bai et al., 2020; Miller-Vedam et al., 2020; O'Donnell et al., 2020; Pleiner et al., 2020), and GET1 (McDowell et al., 2020). All share a conserved core of three TMHs and a cytoplasmic helical hairpin. With YidC also present in the plastid (Alb3; Sundberg et al., 1997) and mitochondrial inner membranes (Oxa1; Bauer et al., 1994; Bonnefoy et al., 1994), it appears that every membrane equivalent to the plasma membrane of the cenancestor contains Oxa1 superfamily proteins. As with SecY, archaeal and bacterial YidC are highly divergent and monophyletic (Anghel et al., 2017; Yen et al., 2001), suggesting that YidC was present alongside SecY in the cenancestor.

Like SecY, YidC facilitates IMP integration by translocating extracytoplasmic segments across the membrane (Borowska et al., 2015; Hell et al., 2001; Samuelson et al., 2000). Unlike SecY substrates however, YidC substrates are limited in the length of polypeptide translocated, typically to less than 30 amino acids (Shanmugam et al., 2019). This limitation may be due to YidC's lack of

a membrane-spanning hydrophilic pore; instead, YidC structures show a membrane-exposed hydrophilic groove that only penetrates partway into the membrane (Kumazaki et al., 2014). YidC therefore forms a partial channel, and may also thin and distort the adjacent membrane (Chen et al., 2017).

The two halves of SecY are structurally similar and related by a two-fold rotational ($C_2$) pseudosymmetry axis which bisects the membrane plane (Van den Berg et al., 2004; Figure 1b). Such pseudosymmetry is common among membrane proteins and arises when the gene encoding an asymmetric progenitor undergoes duplication and fusion (Forrest, 2015). Channels are particularly likely to have a membrane-bisecting $C_2$ axis of structural symmetry because they have the same axis of functional symmetry: they facilitate bi-directional substrate diffusion across the membrane. Indeed, polypeptides can slide through SecY bidirectionally (Ooi and Weiss, 1992), with unidirectionality arising from other factors (Erlandson et al., 2008; Matlack et al., 1998). This symmetry requires that the fused domains be antiparallel, and thus they typically derive from progenitors that existed as antiparallel homodimers (Lolkema et al., 2008; Rapp et al., 2006).

The ubiquity and essentiality of the SecY channel motivated us to investigate how it might have evolved. We identify several structural elements that are conserved between its two halves, which suggest that the SecY progenitor was an anti-parallel homodimer featuring a symmetric pore ring at its dimerisation interface. Automated database searches for structures similar to the SecY halves show that they are uniquely similar to the Oxa1 superfamily. Structural alignments indicate that key residues of YidC's hydrophilic groove and its capping hydrophobic residue are homologous to key residues in SecY's hydrophilic funnels and its pore ring, respectively.

In light of this new correspondence, we re-evaluate the extensive mechanistic literature on SecY and the Oxa1 superfamily, identifying surprising similarities and specific structural bases for their differences. Based on this analysis, we propose that SecY evolved from a dimeric Oxa1 superfamily member by gene duplication and fusion. We compare the range of substrates that can be translocated by YidC to the prokaryotic membrane proteome, and find that a YidC-dependent, SecY-independent cell is plausible. We discuss the implications of this model for the evolution of YidC itself and other components of the general secretory pathway.

## Results

### Conserved pre-duplication features in SecY

Features shared by both of SecY's halves are likely to have been present in their last common ancestor, which we term proto-SecY. In an attempt to identify conserved sequence features of proto-SecY, we aligned the amino acid (a.a.) sequences of a set of N- and C-halves. However, their pairwise identities are just 12.5 ± 2.2% (s.d.), compared to 9.3 ± 4.3% between randomly shuffled sequences, an excess identity of only 6 a.a. per 200 a.a. half. By pairwise HHpred (Zimmermann et al., 2018), the halves have similarity $p = 0.02$, where $p$ estimates the likelihood of observing as much similarity between a random pair of unrelated proteins (Remmert et al., 2012; Söding, 2005). For context, this means that in searching a proteome of ~$10^4$ entries with one half of SecY, one would expect to find ~200 unrelated proteins just as similar as the other half of SecY. Reconstructing a cenancestral SecY sequence using methods previously successful for a different internally duplicated protein (Longo et al., 2020) yielded no increase in similarity between the SecY

halves (see Supplementary Note). Thus, the two halves of SecY have diverged too far from one another to reliably reconstruct proto-SecY's primary sequence.

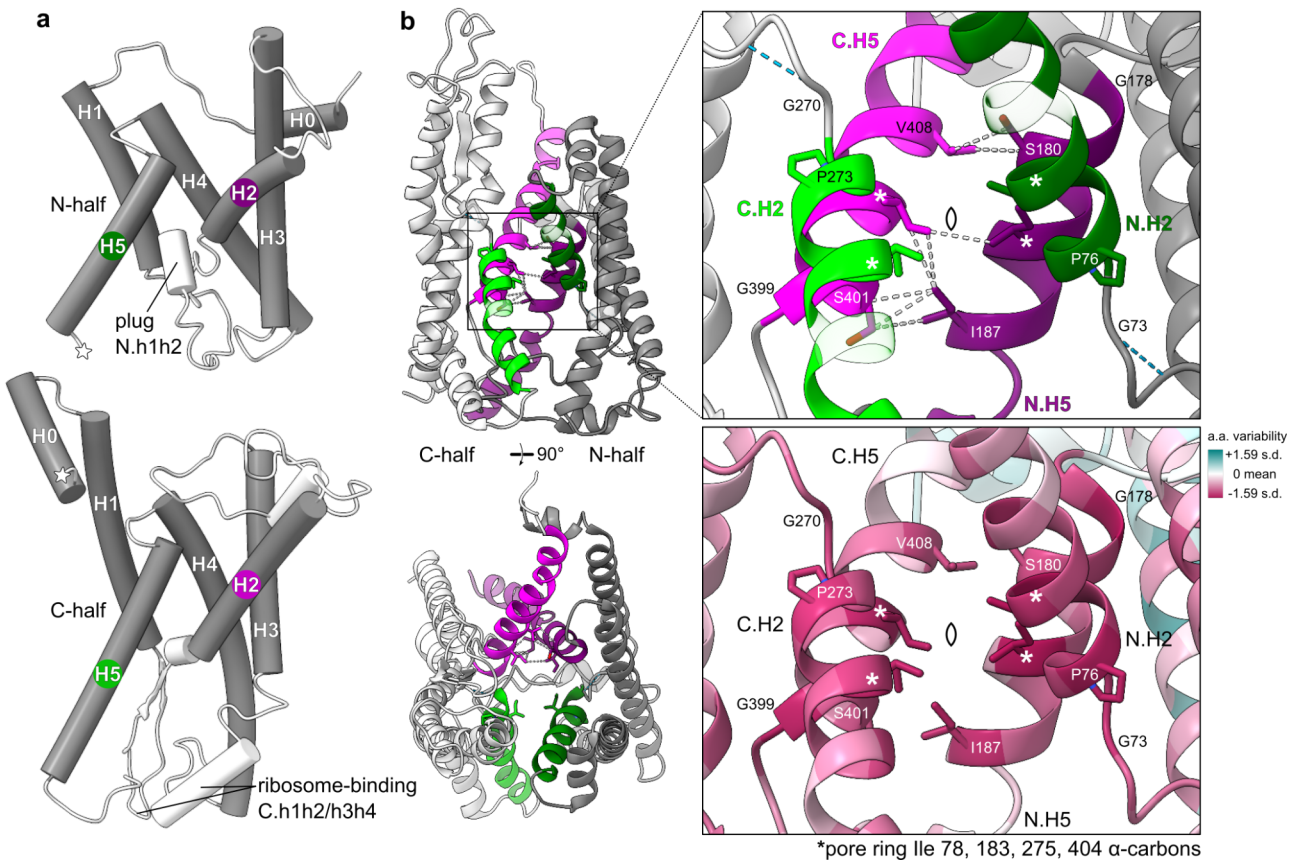


**Figure 2.** Features conserved between SecY's halves. **a** Consensus secondary structure elements (grey) in *Methanocaldococcus jannaschii* SecY (1rhz). Stars indicate where the halves were split. **b** Symmetric features in the most self-similar SecY structure (6itc). A pointed oval indicates the pseudo-$C_2$ symmetry axis. Dashed lines indicate hydrogen bonds (blue) and Van der Waals contacts (white). ConSurf variability scores for an alignment of the N- and C-half sequences are shown mapped onto each half's model. The colour scale encompasses the minimum but not maximum score. The most conserved residues are shown as sticks and labelled.
**Figure 2-Figure supplement 1.** Structural similarity and symmetry breaking between SecY halves.
**Figure 2-Source data 1.** Structure-guided sequence alignment of the SecY halves.

Unlike primary sequence, a five-TMH tertiary structure is conserved by both halves of SecY (Figure 1b; Van den Berg et al., 2004). To facilitate comparisons, we label these five consensus helices H1-H5 (Figure 2a). A prefix of N or C is used when referring to a specific instance of a consensus element in the N- or C-half of SecY. For example, TM6 of SecY is labelled C.H1 because it is located in the C-half and corresponds to H1 of proto-SecY, as does TM1 (N.H1) in the N-half. Flanking and intervening segments are labelled using lower-case references to the nearest consensus elements. For example, the ribosome-binding loop between C.H1 and C.H2 is C.h1h2. The N-terminal peripheral helix of each half, which we argue later was probably also present in proto-SecY, is named H0.

To identify more detailed conserved features, we pursued a precise structural alignment of the SecY halves. We collected a representative set of seven SecY structures: closed (Itskanov et al., 2021; Tanaka et al., 2015), primed (Braunger et al., 2018; Zimmer et al., 2008), and open (Ma et al., 2019; Voorhees and Hegde, 2016) models for eukaryotic and bacterial SecY, and closed archaeal SecY (Van den Berg et al., 2004). The accuracy and extent of pairwise alignments between the halves

from these structures varied widely (Figure 2-Figure supplement 1a), but display one clear trend: the C-halves in the closed and primed structures are least like the N-halves of any structure. This is because closure induces symmetry-breaking tilts in C.H2 and C.H5 (Figure 2-Figure supplement 1b) whereas the N-halves remain relatively unchanged.

Intriguingly, the stability of this asymmetrical closed conformation depends on another asymmetrical feature, the plug (Figure 2a; Li et al., 2007). This suggests that neither the plug nor the closed conformation may have been present in proto-SecY. A plugless proto-SecY is plausible, given that plugless SecY mutants are tolerated (Junne et al., 2006; Park and Rapoport, 2011). If proto-SecY did lack SecY-like gating or a plug, it would then more closely resemble other protein transporters like YidC or TatC, which are not gated (Kumazaki et al., 2014; Rollauer et al., 2012).

The most similar halves, 6fti N (Braunger et al., 2018) and 6itc C (Ma et al., 2019), share a common core (< 4 Å deviation) of 121 a.a. across all 5 helices with 1.9 Å RMSD (Figure 2-Figure supplement 1c). This is precise enough that all 5 helices can be registered unambiguously. Their alignment shows that the four functionally important pore ring residues (Dalal and Duong, 2009) are located at the same two homologous sites in each half. To identify other conserved sites, this structural alignment was then used to align a diverse set of N-half and C-half sequences. Their sequence conservation at each site was then scored and mapped to the most self-similar SecY structure (6itc).

This scored structure shows that the interface between halves is symmetrical and conserved (Figure 2b). N.H5 and C.H5 contact each other via the H5 pore ring residue, which coincides with the symmetry axis, and also via residues -3 and +4 a.a. from the pore ring. Less conserved than the pore ring but still notable are two helix-breaking residues which N-terminate H5 (glycine) and H2 (proline), and a glycine near H2 which bonds its α-hydrogen with the -3 backbone oxygen, thereby stabilising a small bulge. These conserved residues are all within 5 a.a. of the pore ring, underscoring the structural conservation of this central region. Altogether, these features suggest that while proto-SecY may not have had SecY-like gating or a plug, it did form antiparallel homodimers centred on a pore very similar to SecY's. Thus proto-SecY likely functioned as a protein-conducting channel.

## SecY is uniquely similar in structure to the Oxa1 superfamily

With this information about proto-SecY, we sought to identify distant homologs from before its duplication. For this purpose we used Dali, which compares backbone structures and is a top-performing method for remote homolog detection (Holm, 2020). Queries of the PDB with the N- or C-half of SecY yielded a match correlation matrix that indicates the presence of two separate subdomains (Figure 3a). The three-helix bundle of H1/4/5 showed robust self-correlation, but anti-correlation with the H2/3 two-helix hairpin. Because Dali measures global similarity, including both subdomains in our searches would tend to obscure distant homologs which share only one subdomain. We therefore performed searches with not only the whole N- and C-halves, but also their H1/4/5 subdomains (Figure 3b).

After excluding SecY and soluble hits, the highest-scoring hits retrieved by more than one query were members of the Oxa1 superfamily (Figure 3c). Moreover these hits link multiple Oxa1 families (GET1 and EMC3) to both SecY halves, suggesting that their similarity is due to conserved

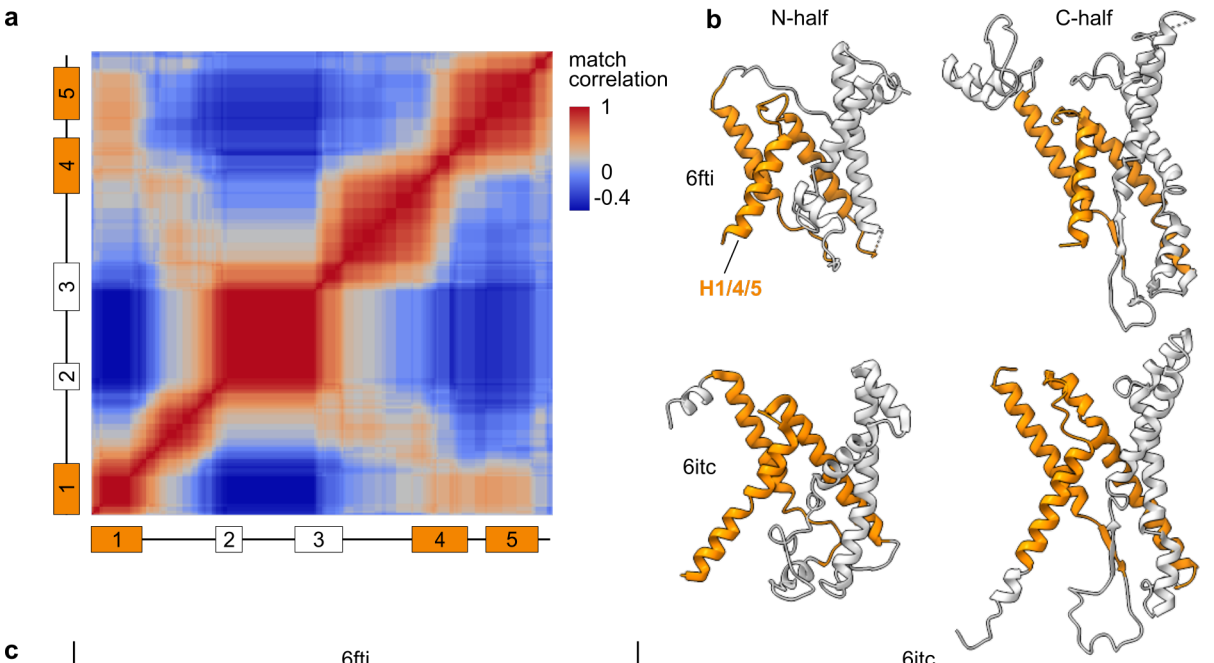


c

| | 6fti | | | | | | | | 6itc | | | | | | | |
|---|---|---|---|---|---|---|---|---|---|---|---|---|---|---|---|---|
| | N | | | | C | | | | N | | | | C | | | |
| Rank | Full | *Z* | H1/4/5 | *Z* | Full | *Z* | H1/4/5 | *Z* | Full | *Z* | H1/4/5 | *Z* | Full | *Z* | H1/4/5 | *Z* |
| 1 | 7d7nA* | 4.5 | **EMC3** | **4.2** | 6xjhA | 4.8 | **EMC3** | **5.6** | 6m49A | 4.0 | 6o84A | 4.8 | 4p6vD | 4.6 | 6qp6A | 5.2 |
| 2 | 2witA | 4.4 | | | 6u0oA | 4.8 | **GET1** | **5.1** | 6z5sW | 3.7 | **GET1** | **4.6** | 6l7oG | 4.4 | **GET1** | **5.0** |
| 3 | **EMC3** | **4.2** | | | **EMC3** | **4.2** | | | **EMC3** | **3.7** | **EMC3** | **4.6** | 4dveA | 4.2 | | |
| 4 | | | | | | | | | | | | | 7d7nA* | 4.1 | | |
| 5 | | | | | | | | | | | | | 5oqkA | 4.1 | | |
| 6 | | | | | | | | | | | | | **GET1** | **4.0** | | |
| SecY | 2ww9A | 15.0 | 2ww9A | 7.7 | 2ww9A | 10.8 | **3bo0A** | **4.0** | 5abbA | 14.3 | 2ww9A | 7.9 | 5abbA | 8.8 | 2ww9A | 5.6 |
| | 3bo0A | 13.8 | 3bo0A | 5.1 | 3bo0A | 10.4 | **2ww9A** | **3.1** | 2ww9A | 13.7 | 3bo0A | 6.1 | 2ww9A | 8.8 | **3bo0A** | **4.0** |
| | 5abbA | 11.8 | **5abbA** | **3.8** | 5abbA | 6.4 | **5abbA** | **2.2** | 3bo0A | 13.0 | **5abbA** | **4.6** | 3bo0A | 8.3 | **5abbA** | **3.1** |

**Figure 3.** SecY's halves are uniquely similar in structure to the Oxa1 superfamily. **a** Match correlation matrix returned by Dali for a half-SecY query (6itc C). The axes are labeled by a diagram of the SecY transmembrane helices. **b** The structural models used as Dali queries. The full models and the H1/4/5 subdomains (orange) were used. **c** Results from querying the PDB25. The top-ranking hits for each query are shown, and any lower-ranking hits that rank higher than the first Oxa1 superfamily hit. Asterisks mark 7d7nA because although it appears twice, those hits are with two non-overlapping parts of the model. Oxa1 superfamily hits are shown by name (EMC3, GET1) instead of PDB code (6ww7C, 6so5C). At bottom are the scores for the SecY hits, which were excluded from the ranking. SecY hits in boldface scored lower than an Oxa1 superfamily hit for that query.
**Figure 3-Figure supplement 1.** Structures of non-Oxa1 superfamily top Dali hits.
**Figure 3-Source data 1**. Results from Dali queries of the PDB25.

characteristics of the Oxa1 superfamily and proto-SecY rather than idiosyncrasies of any one structure. By contrast, all other hits that are as highly ranked are retrieved by only a single query. Manual review of these isolated hits shows them to be obviously dissimilar (Figure 3-Figure supplement 1) due to features ignored by Dali's distance matrix metric, such as gaps, context, and handedness.

To test the sensitivity of these results to our choice of queries (6fti N and 6itc C), selected above for maximum symmetry, we repeated them with the opposite half of each structure (6fti C and 6itc N), with similar results. In the H1/4/5 queries, the Oxa1 superfamily hits rank even higher than some SecY hits, and have Dali *Z*-scores 4.2 to 5.6 standard deviations above the mean, *i.e.* $p = 0.0081$ to 0.0014. It is particularly striking that H1/4/5 of 6fti C retrieves both EMC3 and GET1 with higher *Z*-scores than any SecY structure. Thus, among proteins of known structure, SecY is uniquely

similar to the Oxa1 superfamily.

Moreover, each consensus helix from proto-SecY can be matched to a consensus helix from the Oxa1 superfamily, unambiguously and with the same connectivity (Figure 4, Table 1). The SecY/Oxa1 fold comprises a right-handed three-helix bundle (H1/4/5) interrupted after the first helix by a helical hairpin (H2/3) and prefixed by an N-terminal peripheral helix (H0) which abuts H4 (Figure 4-Figure supplement 1). Thus in addition to sharing a universally conserved core three-TMH bundle, proto-SecY and Oxa1 proteins share a similar composition and connectivity across their full ~200 a.a. lengths.

There is one conspicuous difference between these groups' structures: in SecY, the helical hairpin H2/3 is transmembrane, but in the Oxa1 superfamily it is cytosolic (Figure 4b). If SecY derived from an Oxa1 superfamily ancestor, this would suggest that an initially cytosolic H2/3 evolved to be transmembrane in the proto-SecY stem lineage. Transmembrane hairpins are indeed known to be acquired during membrane protein evolution; convenient examples are provided by the transmembrane hairpins in bacterial YidC h4h5 (Figure 4) and in some SecE (Figure 4-Figure supplement 2).

Starting from a YidC-like H2/3, more membrane-penetrating conformations could have been induced by hydrophobic substitution mutations around the hairpin tip, which lacks conserved hydrophilics (Figure 4-Figure supplement 3). SecY H2/3 could also derive to some degree from indel mutations, particularly since the segment between H1 and H4 is 10 a.a. longer in SecY N than in YidC, and 60 a.a. longer in SecY C. Mutant H2/3 would readily sample membrane-penetrating conformations because it rests at the lipid-water interface (Chen et al., 2017) and is flexibly connected to H1/4/5, as evident in simulations (Chen et al., 2017; Kumazaki et al., 2014) and in the archaeal and bacterial crystal structures where H2/3 was too mobile to be modelled (Borowska et al., 2015; Xin et al., 2018). Because SecY H2/3 is stabilised in the membrane by H1/4/5, it need not have become particularly hydrophobic; for example, most of the H2/3 helices in *G. thermodenitrificans* SecY are predicted to prefer the aqueous phase (N to C: $\Delta G_{app}$ = 1.7, 0.7, 1.0, −1.4 kcal/mol; Hessa et al., 2007).

Late acquisition of the transmembrane H2/3 would explain a curious feature of SecY's structure. H2/3 does not pack against H1 (Figure 4), despite the fact that during co-translational membrane insertion H1 would be exposed to H2/3 without competition. It is reasonable to expect that these elements would interact if their folding pathway had juxtaposed them throughout evolution. This is thought to be why most transmembrane helices pack sequentially against one another (Bowie, 1997; Gimpelev et al., 2004). In SecY however, H1 and H2/3 are separated by H4/5. This suggests that H1/4/5 was the original, sequentially packed transmembrane bundle, and H2/3 only later became transmembrane and packed against its surface. The transmembrane hairpins in bacterial YidC h4h5 and SecE likewise break sequential packing, suggesting that a similar process of transmembrane hairpin acquisition may explain non-sequential TMH packing in other proteins. This is analogous to how RNA branch acquisition left structural fingerprints in the ribosome (Petrov et al., 2014).

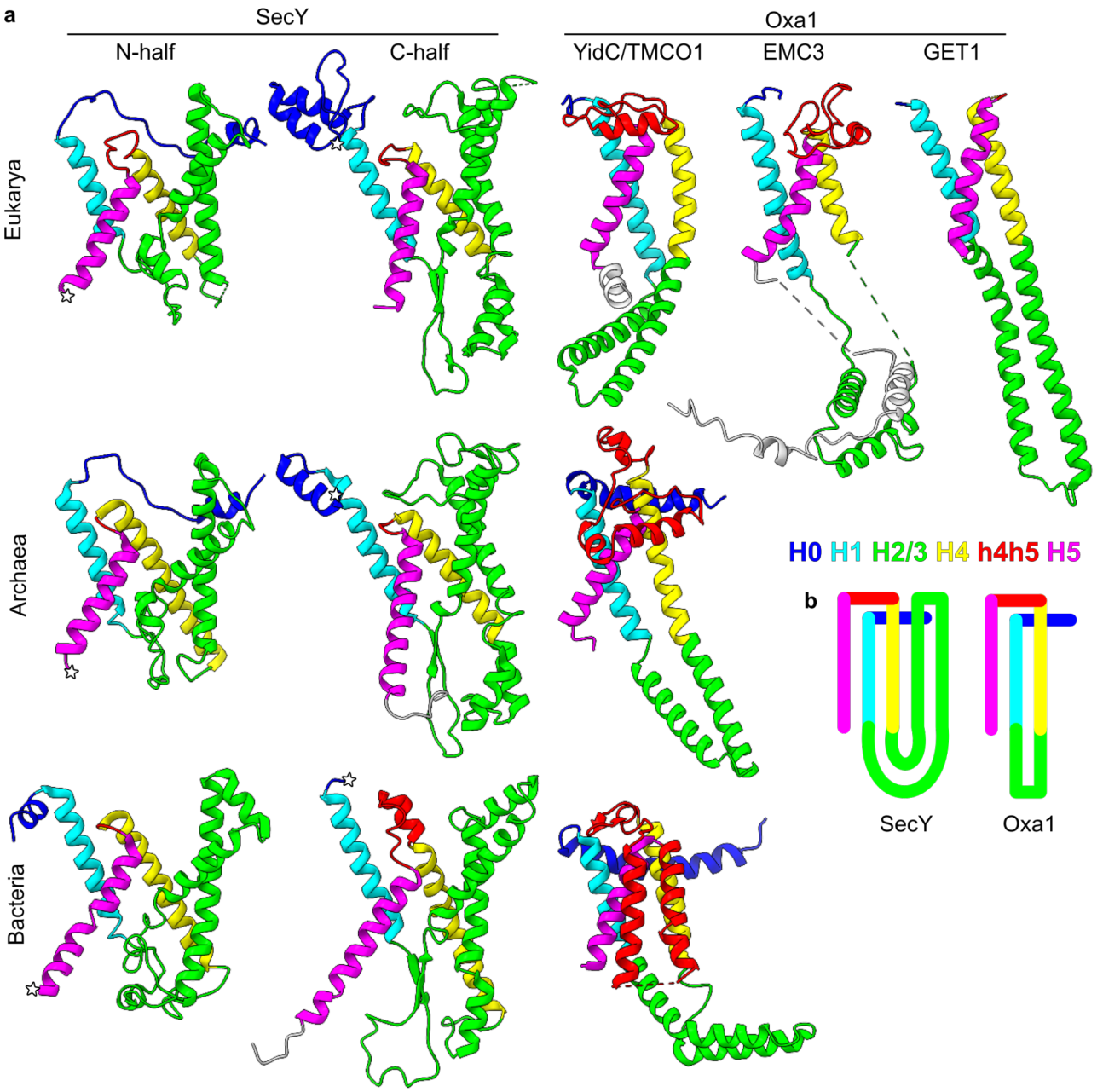


**Figure 4.** Correspondence between structural elements of SecY and the Oxa1 superfamily. Consensus elements and the intervening element h4h5 are coloured according to the key shown. Other intervening elements are coloured to match a neighbouring consensus element, and flanking elements are coloured white. The models are, from left to right and then top to bottom, *Canis lupus familiaris* SEC61A1 (6fti), *Homo sapiens* TMCO1 (6w6l), *H. sapiens* EMC3 (6ww7), *H. sapiens* GET1 (6so5), *M. jannaschii* SecY (1rhz), *M. jannaschii* MJ0480 (5c8j, extended by structure prediction to include the originally unmodelled H2/3; see Figure 4-Figure supplement 4), *G. thermodenitrificans* SecY (6itc), *Bacillus halodurans* YidC2 (3wo6).
**Figure 4-Figure supplement 1.** Structural comparison of H0 in SecY and YidC.
**Figure 4-Figure supplement 2.** Structure of the acquired transmembrane hairpin in SecE.
**Figure 4-Figure supplement 3.** Amino acid conservation in bacterial YidC.
**Figure 4-Figure supplement 4.** Crystallised and predicted structures of archaeal YidC.
**Figure 4-Source data 1.** Predicted structures of archaeal YidC.

Thus SecY and the Oxa1 superfamily have backbone structures that not only are uniquely similar by standard measures, but also could plausibly descend from a common ancestor. This identifies the Oxa1 superfamily as the best candidate for the origin of SecY. The following sections analyse their similarities and differences in mechanistic and functional terms, with a focus on archaeal and bacterial YidC, which would be the closest relatives to SecY.

**Table 1.** Consensus nomenclature for SecY and YidC.

| | SecY | | Consensus structure element | YidC | | | |
|---|---|---|---|---|---|---|---|
| | | | | Archaea-Eukarya | Bacteria | | |
| | | Domain | | | Monoderms & atypical diderms | Diderms* | |
| | | | h0 | | | TM1, P1 | |
| | | | H0 | EH1 | EH1 | EH1 | |
| | TM1 | | H1 | TM1 | TM1 | TM2 | |
| Plug | TM2a | | h1h2 | | | | |
| Lateral gate | TM2b | N | H2 | CH1 | CH1 | CH1 | C1 |
| | TM3 | | H3 | CH2 | CH2 | CH2 | |
| | TM4 | | H4 | TM2 | TM2 | TM3 | |
| | | | h4h5 | EH2 | TM3/4 | TM4/5 | |
| | TM5 | | H5 | TM3 | TM5 | TM6 | |
| | | | h0 | | | TM1, P1 | |
| | | | H0 | EH1 | EH1 | EH1 | |
| | TM6 | | H1 | TM1 | TM1 | TM2 | |
| | C4 | | h1h2 | | | | |
| Lateral gate | TM7 | C | H2 | CH1 | CH1 | CH1 | C1 |
| | C5 | | h2h3 | | | | |
| Lateral gate | TM8 | | H3 | CH2 | CH2 | CH2 | |
| | TM9 | | H4 | TM2 | TM2 | TM3 | |
| | | | h4h5 | EH2 | TM3/4 | TM4/5 | |
| | TM10 | | H5 | TM3 | TM5 | TM6 | |

CH, cytoplasmic helix; EH, extracytoplasmic helix; P, periplasmic domain; C, cytoplasmic domain
*Not all diderms contain a TM before the periplasmic domain P1.

## Corresponding elements of SecY and YidC are mechanistically similar

YidC's hydrophilic groove is functionally similar to those recently observed in components of the retrotranslocation machinery for ER-associated degradation (ERAD; Wu et al., 2020). There, the membrane proteins Hrd1 and Der1 each display hydrophilic grooves, which are open to the cytosol and ER lumen, respectively. The juxtaposition of these two partial channels forms a nearly continuous hydrophilic pore, interrupted by only a thin membrane through which polypeptide translocation is thought to occur. A YidC homolog that formed antiparallel homodimers could similarly create a near-complete channel by juxtaposing two grooves, one on each side of the membrane. Adaptation could then yield the complete channel of proto-SecY.

In both YidC and SecY, the hydrophilic translocation interface is lined by H1/4/5 (Figure 5a). Both three-TMH bundles have a right-handed twist, with H1 and H4 near parallel and H5 packing crossways against them. Of the three helices, it is this crossways H5 that makes the closest contacts with the translocating hydrophilic substrate in both SecY (Figure 5b) and YidC, as determined by chemical crosslinking experiments in *E. coli* (He et al., 2020). These crosslinking data also indicate that YidC's substrates initiate translocation as a hairpin with both termini in the cytoplasm (Figure 5a), just as SecY's substrates do (Mothes et al., 1994; Shaw et al., 1988).

The YidC and SecY H1/4/5 bundles are structurally similar enough that they can be aligned unambiguously (Figure 6a). This alignment superimposes the pore ring residue in SecY H5 onto a conserved hydrophobic residue in YidC H5 that marks the end of the hydrophilic groove. Although in SecY C this hydrophobic residue is at a different position in the membrane compared to YidC, in SecY N its position is similar to an inverted YidC's (Figure 6b), suggesting that the C-half has

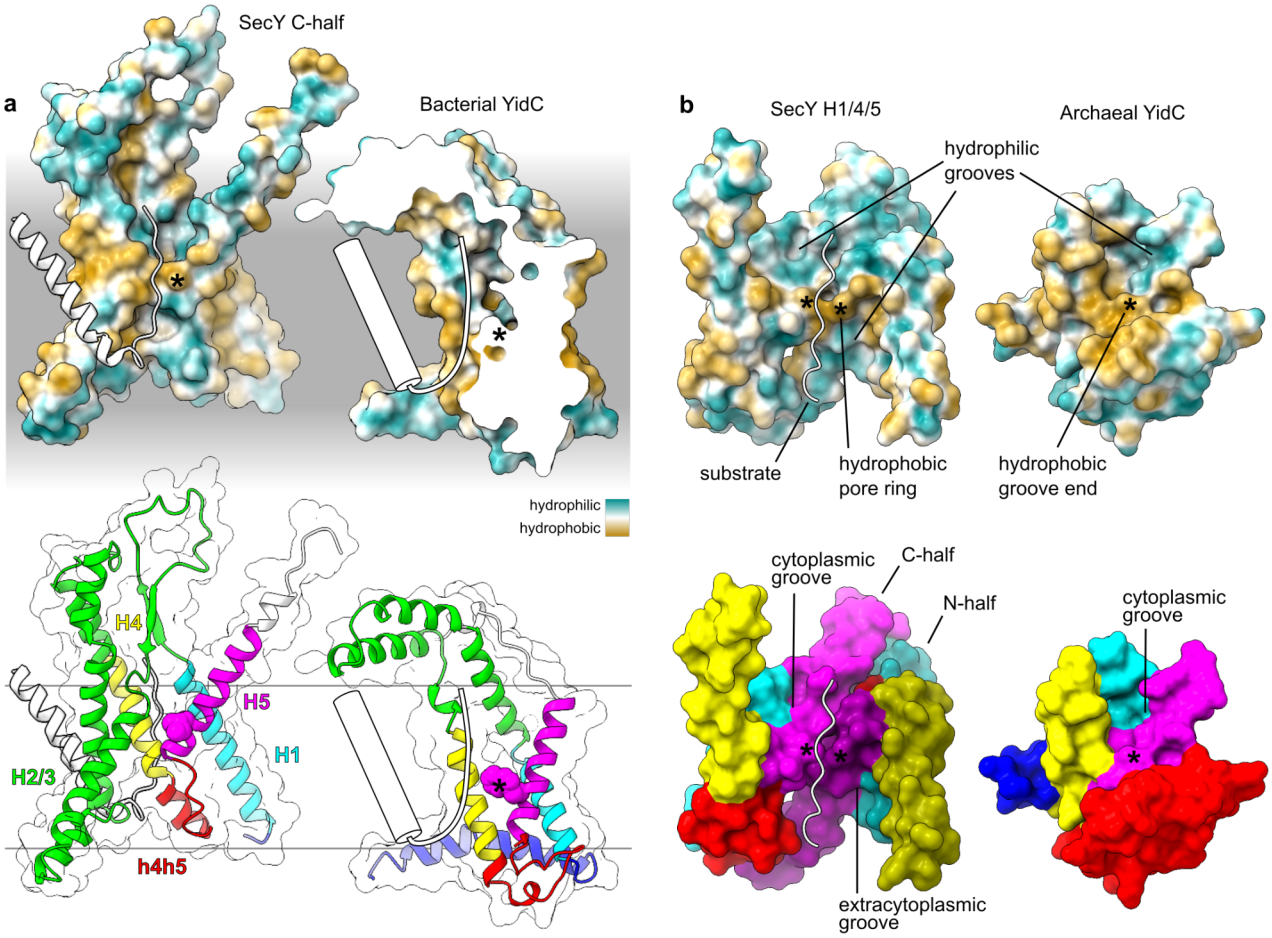


**Figure 5.** Structural and mechanistic comparison of SecY and YidC. The SecY/substrate model is *G. thermodenitrificans* SecY/proOmpA (6itc). **a** Comparison between the SecY C-half (left) and *B. halodurans* YidC2 (right; 3wo7A). The H5 pore ring and the groove end residue are both indicated by asterisks. The hydropathy of the aqueous and lipidic phases ranges from hydrophilic (white) to hydrophobic (grey). Models are oriented and positioned relative to the membrane as described in Methods. A cartoon substrate signal and translocating polypeptide is superimposed on YidC2 to indicate the experimentally determined interface across which substrates translocate and hairpin conformation in which they do so (He et al., 2020). The YidC2 surface and model are clipped to allow a lateral view of the hydrophilic groove which would otherwise be occluded by the bacteria-specific h4h5 transmembrane hairpin (*B. halodurans* YidC2 TM3/4). **b** Left: Lateral view of the SecY/substrate complex showing only the H1/4/5 core of each half. Right: archaeal YidC (*M. jannaschii* MJ0480, 5c8j) in the same relative orientation as SecY.

shifted (~1 nm toward the cytoplasm). In bacterial YidC this groove end residue is aromatic and intimately contacts the bacteria-specific h4h5 hairpin, but in archaeal YidC this residue is aliphatic and most often an isoleucine, just as it is in SecY (Figure 6c). Moreover, the same surrounding positions on H5 are polar (-3, +3, +7, +11) or polarisable aromatics (-1) in both YidC and SecY. Together with a conserved polar residue in H1, these comprise the entire hydrophilic groove of archaeal YidC, and thus that entire groove is also hydrophilic in SecY. Finally, a conserved tryptophan is positioned at the predicted lipid-water interface, which is tryptophan's preferred environment (Yau et al., 1998).

Across the 40 structurally aligned sites, YidC and SecY have 22.5% identical consensus sequences, compared to 30.0% between the SecY halves at these same sites. This detailed similarity in both sequence and structure indicates that the residue at the end of YidC's hydrophilic groove is homologous to the pore ring residue at the end of SecY's hydrophilic funnel. Hydrophobic interactions between these residues in two antiparallel YidC-like monomers would have favoured dimers with a symmetry that juxtaposed them, allowing them to ultimately form the proto-SecY pore ring.

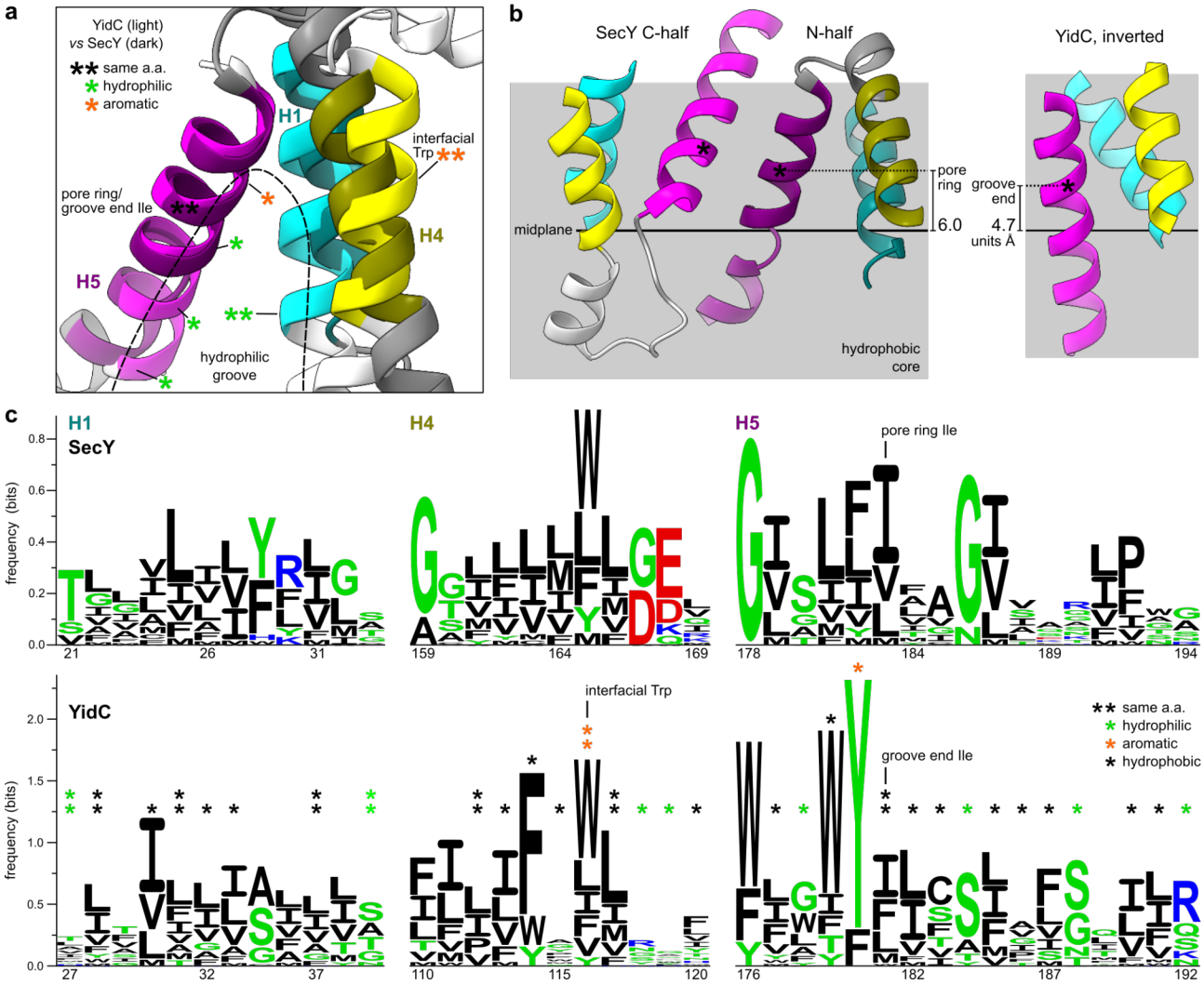


**Figure 6.** YidC and SecY have similar sequence profiles. **a** Superposition of the SecY N-half (*G. thermodenitrificans*, 6itc) and YidC (*M. jannaschii* MJ0480, 5c8j). Coloured segments correspond to the sequence logos in panel c. Some of the residues which are similar in both families are indicated by asterisks, with lines pointing to the corresponding α-carbon. **b** Transmembrane position of the H5 pore ring or groove end residue in the SecY N-half (*G. thermodenitrificans*, 6itc) and YidC (*B. halodurans* YidC2, 3wo7). The boundaries and midplane of the membrane were determined as described in the Methods. **c** Sequence logos for the structurally aligned regions of SecY and archaeal YidC. Column numbers correspond to positions in the proteins modelled in panel a.

## SecY's structural differences from YidC support its unique secretory function

Whereas the conserved cores of SecY and YidC are similar, their differences are concentrated in regions which are hypervariable among the Oxa1 superfamily: h4h5 and H2/3 (Figure 4). H2/3 forms a relatively compact cytosolic hairpin in YidC, is markedly elongated and rigid in GET1, is tethered via long flexible loops in EMC3, and is retained in a roughly similar architecture in TMCO1. By contrast, the H2/3 hairpin in SecY is folded back toward the H1/4/5 bundle and embedded in the membrane.

Despite their differences, H2/3 is a site for substrate signal recognition in both SecY (Figure 7a) and the Oxa1 superfamily. In YidC, TMCO1, and EMC3, the membrane-facing side of H2/3 is thought to interact with substrate TMHs before they reach the hydrophilic groove (Borowska et al., 2015; Kumazaki et al., 2014; McGilvray et al., 2020; Pleiner et al., 2020). In contrast to direct TMH interaction, the rigid and elongated H2/3 coiled coil of GET1 (McDowell et al., 2020) forms a

binding site for the substrate targeting factor GET3 (Mariappan et al., 2011; Stefer et al., 2011; Wang et al., 2011). This adaptation may be due to the particularly hydrophobic TMHs inserted by this pathway (Guna and Hegde, 2018), warranting a specialised machinery to shield them in the cytosol.

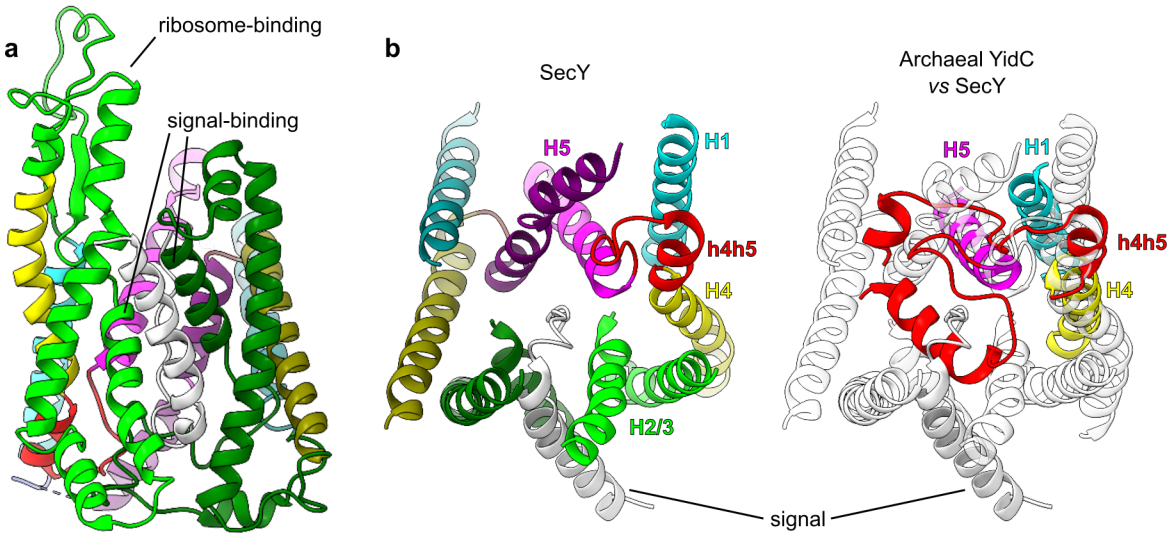


**Figure 7.** Structural features unique to SecY which enable signal binding and substrate translocation. SecY is *G. thermodenitrificans* SecY/proOmpA (6itc). **a** Signal-binding and ribosome-binding sites on SecY H2/3, viewed laterally. **b** The substrate translocation channel, viewed from its extracytoplasmic side. Only H1-5 and h4h5 of SecY are shown. SecY is colour-coded by consensus element as in Figure 4 (left), or rendered transparent and superimposed by the corresponding elements of archaeal YidC *(M. jannaschii* MJ0480, 5c8j), aligned to the SecY C-half (right).

The migration of H2/3 into the membrane in SecY encloses the translocation channel which in YidC is exposed to the membrane (Figure 7b). This allows SecY to create a more hydrophilic and aqueous environment for its hydrophilic substrates, facilitating their translocation. This is particularly important for SecY's secretory function, which involves translocating much longer hydrophilic segments than those translocated by YidC.

As a secondary consequence, transmembrane insertion of H2/3 makes the site where signals initiate translocation more proteinaceous and hydrophilic (Figure 5a; Gogala et al., 2014; Park et al., 2014; Plath et al., 1998; Voorhees and Hegde, 2016; Weng et al., 2020). Because of this, translocation via SecY can be initiated via signals which are much less hydrophobic than the TMHs which initiate translocation via YidC. This, too, is important for SecY's secretory function, because the signal peptides of secretory proteins are distinguished from TMHs by their relative hydrophilicity (von Heijne, 1985). This biophysical difference allows signal peptidase to specifically recognise and cleave them (Paetzel et al., 2002). Cleavage frees the translocated domain from the membrane to complete secretion.

After H2/3, the next most conspicuous difference between SecY and YidC is in h4h5, which is nearly absent from SecY (Figure 7b). Whereas the H2/3 transmembrane insertion differentiates how SecY and YidC receive and recognise hydrophobic domains, the absence of h4h5 clears the channel through which hydrophilic substrates translocate. As mentioned previously, h4h5 is, like H2/3, hypervariable in the Oxa1 superfamily, forming a peripheral helix in archaea and eukaryotes and a transmembrane hairpin in bacteria. If a more YidC-like h4h5 were present in proto-SecY, proto-SecY dimerisation would place h4h5 inside the hydrophilic groove of the opposite monomer,

instead of in contact with the membrane. Thus a YidC-like h4h5 would be selected against in SecY, to maintain a membrane-spanning hydrophilic pore and facilitate translocation.

### Like proto-SecY, YidC uses the distal face of H5 for dimerisation

As shown above, it appears that proto-SecY formed antiparallel homodimers via the distal face of H5 (Figure 8a); here we consider whether this characteristic could have arisen in an ancient member of the Oxa1 superfamily. Antiparallel homodimerisation requires that the monomer possess two characteristics: a tendency to be produced in opposite topologies, and an interface suitable for dimerisation. Although dual-topology is not evident in the Oxa1 superfamily, distant ancestors could easily have had this property with relatively few changes. Making only a few changes to basic amino acids (especially lysine and arginine) flanking the first TMH of an IMP can influence its topology, and an inverted first TMH can invert an entire IMP containing several TMHs (Beltzer et al., 1991; Brown et al., 2018; Rapp et al., 2006, 2007). Such changes in topology occur naturally in protein evolution (Rapp et al., 2006; Sääf et al., 1999), and YidC does not contain any conserved basic residues in its soluble segments that would impede this evolutionary process (Figure 4-Figure supplement 4). Moreover, the lysine and arginine bias in extant YidC is no greater than that previously observed in proteins which acquir ed divergent orientations (Sääf et al., 1999).

Unlike dual-topology, interactions via the distal face of H5 are known to occur in several Oxa1 superfamily members. This surface forms an intramolecular interaction with the h4h5 transmembrane hairpin in bacterial YidC but remains exposed in archaeal YidC and its eukaryotic homologs (Figure 4). There are no published data on YidC biochemistry in archaeal cells, but eukaryotic EMC3 and GET1 are known to form functionally important complexes, and structural models show that they use the distal face of H5 to do so (Figure 8a; Bai et al., 2020; McDowell et al., 2020; Miller-Vedam et al., 2020; O'Donnell et al., 2020; Pleiner et al., 2020) These interactions via H5 are heterodimeric, rather than homodimeric, but nonetheless demonstrate that EMC3 and GET1 can dimerise (with EMC6 and GET2, respectively) along the same interface as the proto-SecY homodimer without impeding their translocation activities.

To determine whether these H5 interactions are ancient or eukaryote-specific, we queried nine diverse archaeal proteomes for homologs of *H. sapiens* EMC6 or GET2 using HHpred (Zimmermann et al., 2018). Although none displayed significant similarity with GET2, every proteome queried contained exactly one protein similar to EMC6 (Figure 8b). Among these archaeal proteins, those most similar to eukaryotic EMC6 tend to come from the species most closely related to eukaryotes: the Asgard archaean, then the TACK archaean, and then the euryarchaeans. This phylogenetic concordance indicates that the archaeal proteins are homologs of the eukaryotic protein, and that their ubiquity is due to an ancient origin. We provisionally name them Elp1, for EMC6-like protein 1.

Reciprocal queries of *H. sapiens* and *S. cerevisiae* proteomes with the Asgard Elp1 (Lokiarch_50810) identified EMC6 in both cases as high-confidence hits. Unexpectedly, the *H. sapiens* search also identified an even more similar hit, C20orf24 (Figure 8b), which we provisionally name ELP1. These proteins all share a structurally similar three-TMH core (Figure 8-Figure supplement 1a; Figure 8-Figure supplement 2), as evident in both *de novo* and homology-templated structures predicted by trRosetta (Yang et al., 2020).

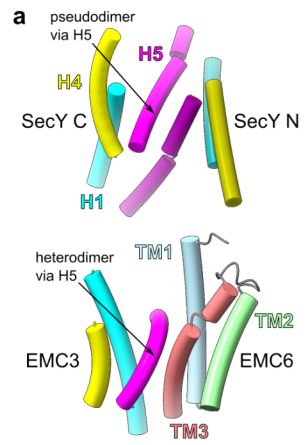


**b**

**Archaeal and eukaryotic EMC6-like proteins (Elp1/ELP1)**

| Query | Proteome | Name | E-value | Phylum |
|---|---|---|---|---|
| *H. sapiens* | *Pyrococcus horikoshii* | hypothetical protein | $4.50\times10^{-16}$ | Euryarchaeota |
| EMC6 | *Lokiarchaeum sp. GC14_75* | h.p. Lokiarch_50810 | $9.20\times10^{-16}$ | Proteoarchaeota (Asgard) |
| | *Saccharolobus solfataricus* | hypothetical protein | $3.60\times10^{-11}$ | Proteoarchaeota (TACK) |
| | *Methanocaldococcus jannaschii* | h.p. MJ0606 | $2.90\times10^{-8}$ | Euryarchaeota |
| | *Archaeoglobus fulgidus* | hypothetical protein | $3.4\times10^{-5}$ | |
| | *Methanosarcina* | hypothetical protein | $6.6\times10^{-5}$ | |
| | *Methanothermus fervidus* | hypothetical protein | $3.9\times10^{-5}$ | |
| | *Thermoplasma acidophilum* | hypothetical protein | $1.5\times10^{-4}$ | |
| | *Halobacterium jilantaiense* | hypothetical protein | $6.5\times10^{-4}$ | |
| | X *H. jilantaiense* | hypothetical protein | 2.3 | |
| Lokiarch _50810 | *H. sapiens* | unc. prot. C20orf24 | $3.80\times10^{-13}$ | |
| | *H. sapiens* | EMC6 | $1.20\times10^{-12}$ | |
| | *S. cerevisiae* | EMC6 | $1.10\times10^{-12}$ | |
| | X *H. sapiens* | EAAT1 | 80 | |

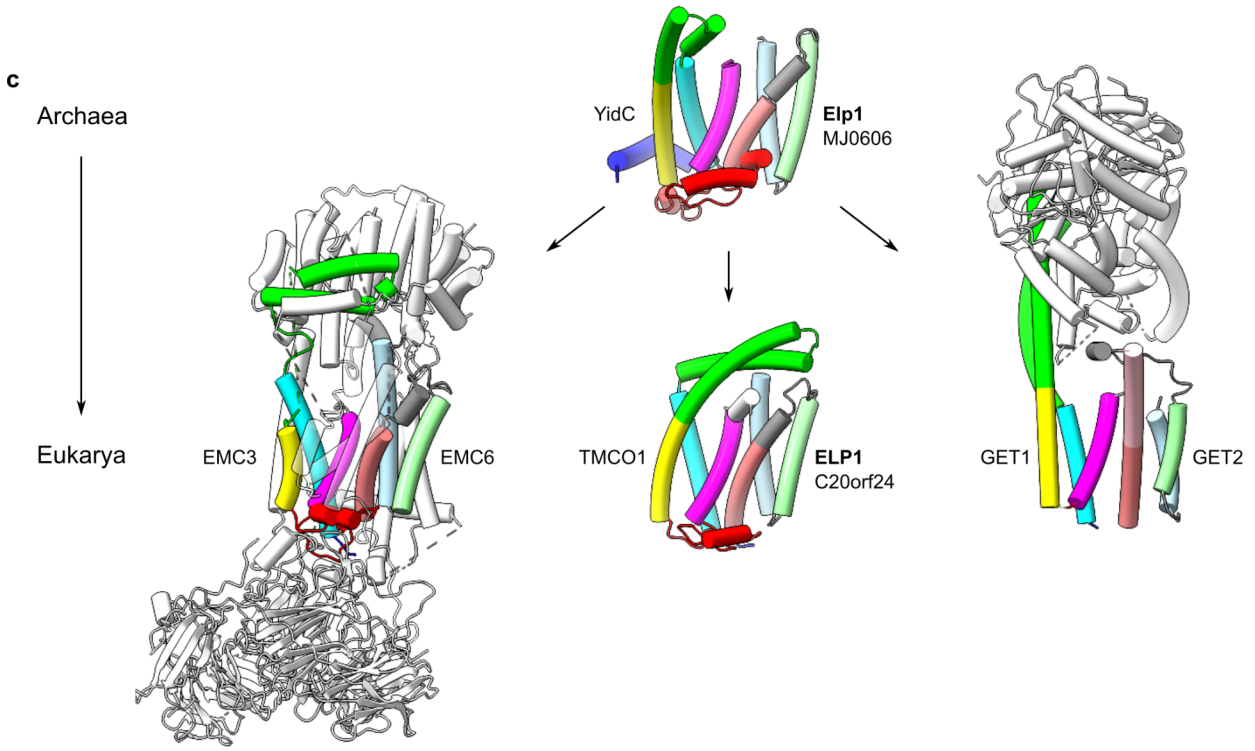


**Figure 8.** Ubiquitous dimers formed by YidC via the same interface as proto-SecY. **a** Comparison of the EMC3/6 and proto-SecY dimerisation interfaces. Models show *S. cerevisiae* EMC3 H1/4/5 with EMC6 (6wb9) and *G. thermodenitrificans* SecY H1/4/5 (6itc). **b** Archaeal and eukaryotic HHpred hits. A red cross and grey text indicates the first rejected result. For sequence accession numbers, see Methods. **c** Structural models of the archaeal and eukaryotic heterodimers of YidC and EMC6/GET2 homologs. *S. cerevisiae* EMC (6wb9) and *H. sapiens* GET1/2/3 (6so5) are shown. The N-terminal half of GET2 TM3 which is identified as a sequence insertion by alignment to Elp1 is shown in pink. The *M. jannaschii* YidC/Elp1 (MJ0480/MJ0606) models were predicted by trRosetta and aligned to the EMC3/6 dimer. The *H. sapiens* TMCO1/ELP1 dimer is represented similarly, except the TMCO1 model is from the PDB (6w6l).
**Figure 8-Source data 1.** Structure and contact predictions for the EMC6-like proteins.
**Figure 8-Figure supplement 1.** Structure and contact prediction for archaeal and human EMC6-like proteins.
**Figure 8-Figure supplement 2.** Structural models for nine diverse archaeal EMC6-like proteins.

The patterns of co-evolution between archaeal YidC and Elp1 showed that their highest-probability contacts all occur along the same interface used for dimerisation by eukaryotic EMC3/6 (Figure 8-Figure supplement 1b). This indicates that the distal face of H5 is used for heterodimerisation not only by eukaryotic EMC3 and GET1 but also by archaeal YidC. The third eukaryotic Oxa1 family, TMCO1, displays a similar pattern of co-evolution with ELP1, indicating that they form a similar heterodimer (Figure 8-Figure supplement 1b). TMCO1-ELP1 interaction is consistent with the absence of ELP1 from *S. cerevisiae* (Figure 8b), because it also lacks TMCO1.

Although GET2 lacks strong sequence similarity with these EMC6 homologs, its structural similarity with EMC6 was immediately recognised (McDowell et al., 2020; Pleiner et al., 2020). Our identification of archaeal EMC6 homologs reveals a plausible origin for GET2. Consistent with this, although our GET2 query of the lokiarchaean proteome did not identify any very high-similarity proteins, the most similar membrane protein was indeed Elp1 (Lokiarch_50810, HHpred $p = 0.0057$). Moreover, the aligned columns between GET2 and Elp1 correspond exactly to their structurally similar transmembrane domains. The single large gap in this alignment spans the cytosolic extension of GET2 TM3, which brings it into contact with GET3 (Figure 8c). Thus, the major difference between GET2 and EMC6 can be explained as a functional adaptation for GET3 recognition, not unlike GET1's elongation of H2/3.

The absence of a similar heterodimer in bacteria suggests that it may have been acquired in archaea after divergence from bacteria, which instead acquired the H5-occluding transmembrane hairpin in h4h5 (Figure 4). An archaeal origin for Elp1 would be consistent with its genomic location, which is distant from the widely conserved cluster of cenancestral ribosomal genes, SecY and YidC (Makarova et al., 2015). In the period prior to heterodimerisation with Elp1, a YidC homolog could have evolved to use H5 for homodimerisation, giving rise to proto-SecY. YidC's universal tendency to cover the distal face of H5 supports this possibility.

## Reductive selection in symbionts demonstrates the functional range of YidC

If proto-SecY originated in the YidC family, YidC might initially have been the cell's only transporter for the extracytoplasmic parts of IMPs. But some IMPs cannot be integrated by YidC, and instead depend on SecY (Welte et al., 2011). Thus a cell with YidC and not SecY may have been constrained to express a more limited range of IMPs. The looser this constraint, the more plausible it is that such a cell would be viable, and that YidC could have preceded SecY.

Insight into this question of *in vivo* sufficiency can be obtained by inspection of the only cells known to have survived SecY deletion: the mitochondrial symbionts. SecY has been lost from all mitochondrial genomes for which sequences are available, except in one group of eukaryotes, and it has not been observed to relocate to the nuclear genome (Janouškovec et al., 2017). The exceptional group is the jakobids, only a subset of which retain SecY. The incomplete presence of SecY in this group implies that SecY was lost multiple times from the jakobids and their sister groups. SecY deletion is therefore a general tendency of mitochondria, rather than a single deleterious accident.

Mitochondria retain two YidC homologs, Oxa1 and Oxa2 (Cox18), the genes for which relocated from the mitochondrial genome to the nuclear genome (Bauer et al., 1994; Bonnefoy et al., 1994). As nuclear-encoded mitochondrial proteins, they are translated by cytosolic ribosomes and then imported into mitochondria via channels in the inner and outer mitochondrial membranes (Wiedemann and Pfanner, 2017). These channels are essential for the import of nuclear-encoded proteins, but are not known to function in the integration of mitochondrially encoded IMPs (meIMPs), which instead requires export from the matrix, where they are synthesized by mitochondrial ribosomes. This export is generally Oxa1-dependent (Hell et al., 2001).

The meIMPs have diverse properties, including 1 to 19 TMHs and exported parts of various sizes and charges (Figure 9a-c). Oxa1's sufficiency for their biogenesis *in vivo* is consistent with *in vitro* results showing that *E. coli* YidC is sufficient for the biogenesis of certain 6- and 12-TMH model

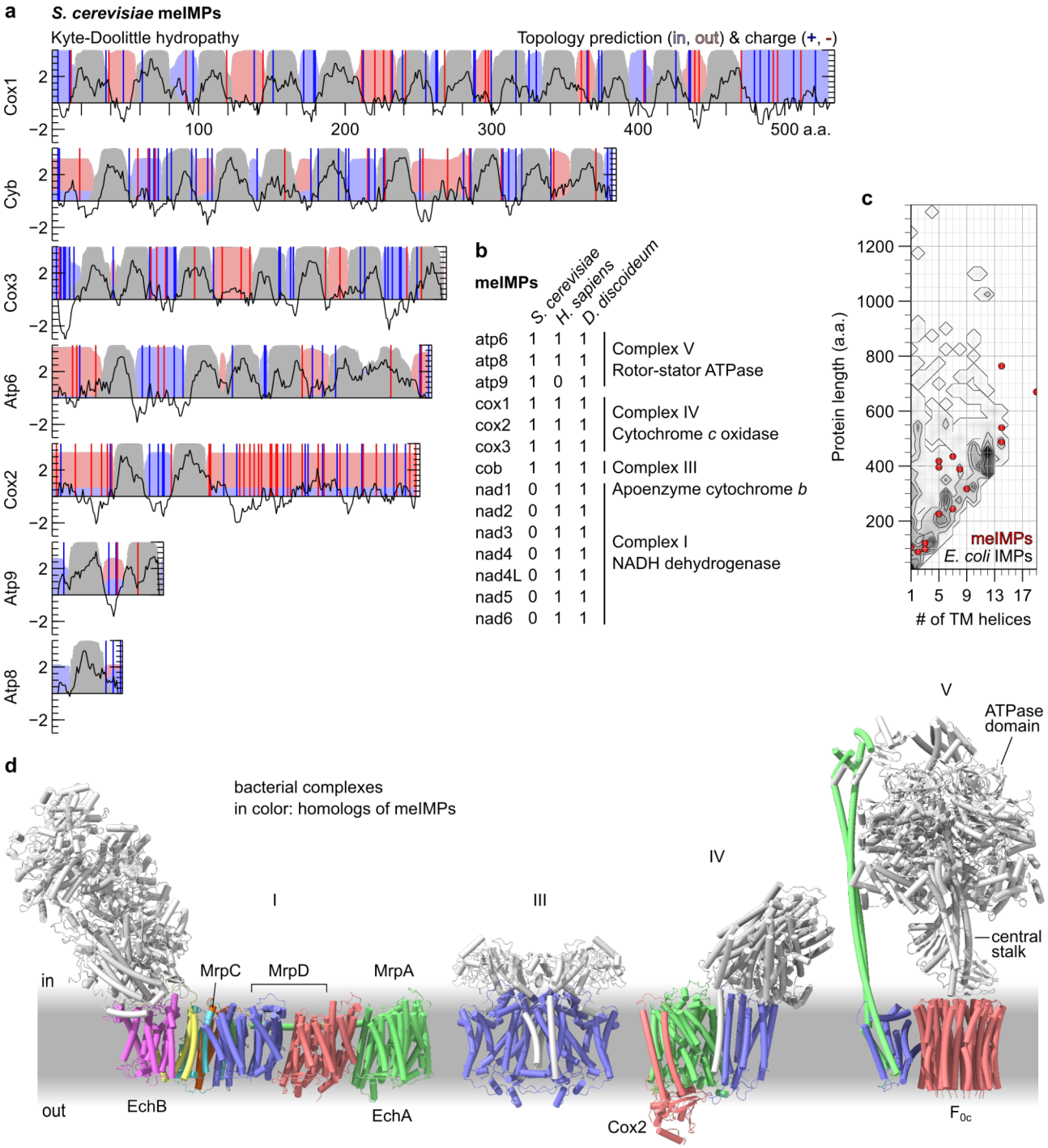


**Figure 9.** Substrates of the mitochondrial SecY-independent pathway for IMP integration. **a** Sequence characteristics of the mitochondrially-encoded IMPs (meIMPs) from *S. cerevisiae*. Kyte-Doolittle hydropathy (left axis) is averaged over a 9 a.a. moving window (black line). Topology predictions were computed by TMHMM (right axis) to indicate regions which are retained in the mitochondrial matrix (light blue field), inserted into the membrane (grey field), or exported to the intermembrane space (light red field). Positive (blue) and negative (red) residues are marked with vertical bars. **b** Table of all meIMPs in a fungus (*S. cerevisiae*), a metazoan (*H. sapiens*) and an amoebozoan (*Dictyostelium discoideum*). **c** Scatter plot of the length and number of TMHs in the meIMPs of a eukaryote (*D. discoideum*), superimposed on a contour plot and heat-map of all 910 IMPs from a proteobacterium (*E. coli;* 170 single-pass, 740 multi-pass). Protein lengths were binned in 25 a.a. increments. Each contour represents an increase of 3 proteins per bin. Protein lengths and TMH counts are from UniProt (The UniProt Consortium, 2019). **d** Structures of prokaryotic complexes homologous to meIMPs. Subunits not homologous to the meIMPs listed in panel b are shown in white. Homo-oligomers are represented by a single colour. From left: I, NADH dehydrogenase (*Thermus thermophilus*, 6y11; Gutiérrez-Fernández et al., 2020), III, cytochrome *bc*1, (*Rhodobacter sphaeroides*, 6nhh; Esser et al., 2019), IV, cytochrome *c* oxidase (*R. sphaeroides*, 1m57; Svensson-Ek et al., 2002), V, rotor-stator ATPase (*Bacillus* sp. PS3, 6n2y; Guo et al., 2019). The labelled subunits of NADH dehydrogenase (I) are homologous to the two IMP subunits of the energy-converting hydrogenase (EchA/B), and/or to subunits of the multiple-resistance and pH (Mrp) antiporters. The labelled subunits of IV and V indicate those referenced in the text.

substrates (Serdiuk et al., 2019; Welte et al., 2011). The only apparent constraint on the meIMPs is that they tend to have only short (~15 a.a.) soluble segments. This is consistent with observations from *E. coli* that fusing long soluble segments to a YidC-dependent IMP can induce SecY dependence (Andersson and von Heijne, 1993; Kuhn, 1988; Shanmugam et al., 2019). Among the meIMPs, Cox2 is an exception which proves the rule, because Oxa1 cannot efficiently translocate its exceptionally long (~140 a.a.) C-terminal tail; instead it is translocated by Oxa2 in cooperation with two accessory proteins (Saracco and Fox, 2002).

This constraint on soluble segment length is less consequential than it may at first appear, because prokaryotic IMPs in general tend to have only short soluble segments (Figure 9c; Wallin and von Heijne, 1998). Thus, most prokaryotic IMPs may be amenable to SecY-independent, YidC-dependent biogenesis. Consistent with this, in *E. coli*, the signal recognition particle (SRP) has been found to target nascent IMPs to either SecY or YidC (Welte et al., 2011), and YidC is present at a concentration 1–2× that of SecY (Schmidt et al., 2016). By contrast, IMPs with large translocated domains became much more common in eukaryotes (Wallin and von Heijne, 1998) concomitant with YidC's divergence into three niche paralogs, none of which are essential at the single-cell level (Guna et al., 2018; Jonikas et al., 2009; McGilvray et al., 2020).

Even without extrapolating from the meIMPs to other similar IMPs, it is clear that chemiosmotic complexes are amenable to YidC-dependent, SecY-independent biogenesis (Figure 9d). These complexes couple chemical reactions to the transfer of ions across the membrane and are sufficient for the membrane's core bioenergetic function. Although the complexes shown participate in aerobic metabolism, which presumably post-dates the oxygenation of Earth's atmosphere, they have homologs which enable chemiosmosis in anaerobes. In particular, chemiosmosis in methanogens and acetogens employs the rotor-stator ATPase, Mrp antiporters, and an energy-converting hydrogenase (Ech; Lane and Martin, 2012), all of which have homologs of their IMP subunits among the meIMPs (Figure 9d) and may have participated in primordial anaerobic metabolism (Weiss et al., 2016).

Thus if YidC had preceded SecY, it would have been sufficient for the biogenesis of diverse and important IMPs, but likely not the translocation of large soluble domains. This is supported by the results of reductive selection in chloroplasts, which retain both SecY (cpSecY) and YidC (Alb3) (Xu et al., 2020). cpSecY imports soluble proteins across the chloroplast's third, innermost membrane, the thylakoid membrane (Peltier et al., 2002). This thylakoid membrane was originally part of the chloroplast inner membrane (equivalent to the bacterial plasma membrane), much like the mitochondrial cristae, but subsequently detached and now forms a separate compartment (Vothknecht and Westhoff, 2001). Because the thylakoid membrane is derived from the plasma membrane, import across the thylakoid membrane is homologous to secretion across the plasma membrane. Thus, when symbiosis removed the need for secretion, SecY was eliminated from mitochondria, whereas it was retained in chloroplasts for an internal function homologous to secretion.

A primordial YidC-dependent cell may simply not have secreted protein or may instead have used a different secretion system. Notably one primordial protein secretion system has been proposed: a protein translocase homologous to the rotor-stator ATPases (Mulkidjanian et al., 2007). Translocases are transporters which use chemical reactions to drive translocation (Tipton, 2018),

such as the translocase formed when the SecA ATPase acts in tandem with the SecYEG channel (Erlandson et al., 2008). The putative rotor-stator-like protein translocase used its ATPase subunit to unfold and feed substrates through the homo-oligomeric channel formed by $F_{0c}$, now occupied by the central stalk (Figure 9d). The strict YidC-dependence of $F_{0c}$ biogenesis in *E. coli* (Yi et al., 2003) hints that they shared an era of co-evolution, as a laterally closed channel for the secretion of soluble proteins ($F_{0c}$) and a laterally open channel for the integration of membrane proteins (YidC), including $F_{0c}$ itself. The subsequent advent of a laterally gated channel, SecY, would have facilitated the biogenesis of a hybrid class of proteins: IMPs with large translocated domains.

## Discussion

By comparing structures of the SecY N- and C-halves, we identified a maximum-symmetry pair, and thus an estimate of the structure of their last common ancestor, proto-SecY. Their alignment identifies homologous sites in each half, revealing that both the hydrophobic pore ring and the interface between halves are symmetric. The conservation of these features indicates that they were also present in proto-SecY, and thus that it formed antiparallel homodimers and functioned as a protein-conducting channel.

In automated database searches for structures similar to SecY's halves, the top hit is the Oxa1 superfamily, of which YidC is the prokaryotic member. The SecY/Oxa1 fold consists of a right-handed three-helix bundle (H1/4/5), interrupted after the first helix by a helical hairpin (H2/3) and prefixed by an N-terminal peripheral helix (H0) that abuts H4. The H2/3 hairpin is cytosolic in the Oxa1 superfamily but transmembrane in SecY, where it forms the lateral gate helices. This suggests that H2/3 was originally cytosolic, then evolved to pack against the surface of H1/4/5 in the proto-SecY stem lineage. This sequence of events would explain the peculiar non-sequential packing arrangement of SecY's transmembrane helices.

This unexpected correspondence motivates a re-evaluation of the literature on SecY and YidC. In both, H1/4/5 buries a hydrophilic groove inside the membrane to facilitate the translocation of hydrophilic polypeptide. Juxtaposing two grooves, one on each side of the membrane, allows SecY to open a membrane-spanning pore, whereas YidC has only a cytoplasmic groove. Structural alignments superimpose the hydrophobic residue in H5 that rings the SecY pore onto the hydrophobic residue that ends the YidC groove, and likewise the surrounding polar and aromatic groove residues. Both SecY and YidC recognise hydrophobic helices in their substrates via binding at the protein-lipid interface, and in doing so induce a hairpin conformation in the substrate's hydrophilic flank which initiates its translocation. The SecY-specific lateral gate helices create a more hydrophilic environment for signal recognition and substrate translocation that is better suited to SecY's specific secretory function.

Whereas proto-SecY formed homodimers via the distal face of H5, two of the three eukaryotic Oxa1 member families are known to use this interface for heterodimerisation. Homology would predict that this is an ancient tendency. We indeed found indications that H5-mediated heterodimers are formed by the third eukaryotic Oxa1 superfamily member, TMCO1, and by archaeal YidC. In bacterial YidC this interface instead makes intramolecular contacts with bacteria-specific TMHs. To gauge the plausibility of a YidC-dependent, SecY-independent primordial cell, we reviewed the range of substrates translocated by YidC in SecY-lacking mitochondria, and found that it spans most

of the diversity of the prokaryotic membrane proteome. The surprising conclusion of our study is that a YidC homolog could have both preceded and evolved into proto-SecY, whose gene duplication and fusion then originated the present-day SecY family.

## Evaluation of the homology hypothesis

It is important to consider whether the similarities between SecY and YidC could arise by convergent evolution under shared constraints (making them analogs), rather than divergent evolution from a common ancestor (making them homologs). Deciding between the analogy hypothesis and the homology hypothesis requires an assessment of whether any plausible constraints could explain their similarities (Doolittle, 1994). We will weigh their functional, mechanistic, structural, and sequence similarities in turn.

Laterally open helical protein channels have arisen by functional convergence several times (Figure 10). Thus if the similarity between SecY and YidC were solely functional, the analogy hypothesis would be attractive. Analogy would also be plausible if the similarity between SecY and YidC were solely mechanistic, because their mechanism is common among amphiphile transporters. Many use a membrane-exposed hydrophilic groove to translocate the hydrophilic parts of an amphiphile while

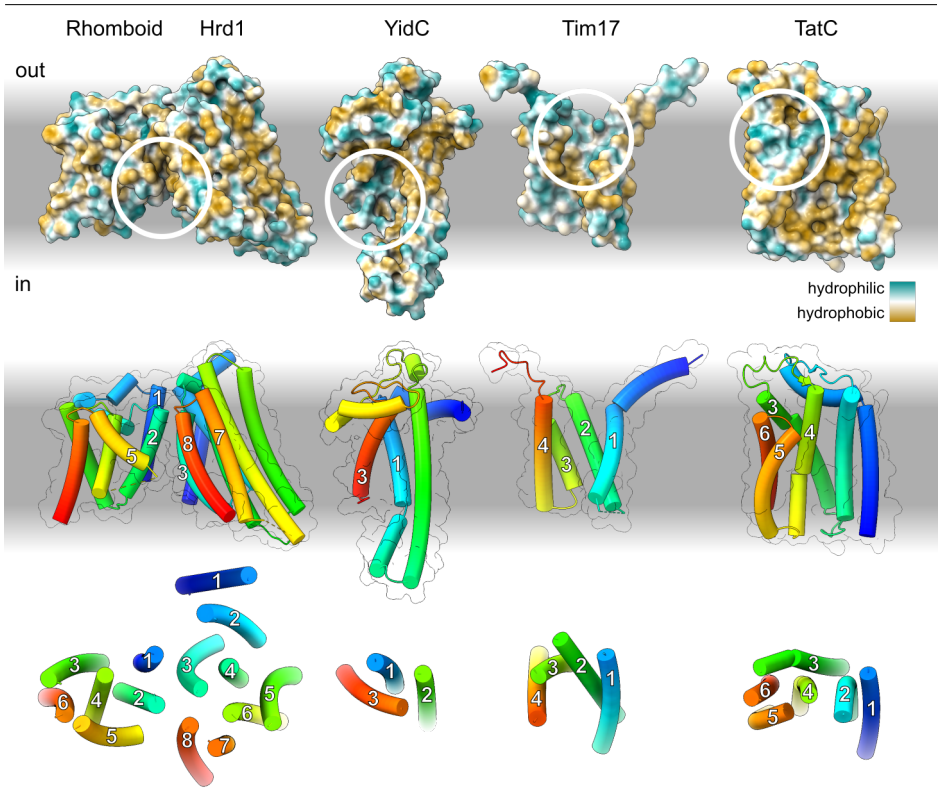


**Figure 10.** Structures of the known families of laterally open helical protein channels. Top: Structural models shown as solvent-excluded surfaces colour-coded by hydropathy. The hydropathy of the lipidic and aqueous phases represented on a separate scale, ranging from hydrophilic (white) to hydrophobic (grey). White circles indicate intramembrane hydrophilic grooves. Middle: models shown as tubes colour-coded by position. Transmembrane segments in the vicinity of the hydrophilic groove are numbered. Bottom: Axial views of each molecule showing only transmembrane helices. From left to right, the models representing each family are as follows. Rhomboid: *S. cerevisiae* Der1 (6vjz), Hrd1: *S. cerevisiae* Hrd1 (6vjz), YidC: *M. jannaschii* MJ0480 (5c8j, extended by structure prediction to include the originally unmodelled H2/3; see Figure 4-Figure supplement 4), Tim17: *S. cerevisiae* Tim22 (6lo8, Zhang et al., 2020), TatC: *Aquifex aeolicus* TatC (4b4a, Rollauer et al., 2012).

exposing its hydrophobic parts to the bilayer (Bakelar et al., 2016; Brunner et al., 2014; McKenna et al., 2020). Moreover the hairpin conformation which protein transporters induce in their substrates is a predictable result of physical constraints which disfavour head-first translocation (Engelman and Steitz, 1981).

Thus there is precedent and a clear physical basis for SecY and YidC's functional and mechanistic similarities arising by convergence. But the same is not true of their structural similarities. First, it would be unprecedented for structural similarity to arise by convergence within this functional class, given that all other known amphiphile transporters are grossly dissimilar from one another, including all other laterally open helical protein channels (Figure 10). This suggests that the space of mechanically sufficient folds is large, and thus the likelihood of convergence low.

Second, the extensive literature on SecY and YidC discussed throughout this paper suggests no physical reason why their mechanism would favour the SecY/Oxa1 fold. Thus attributing their structural similarity to mechanistic constraints would require one to assume that such a constraint exists. On the contrary, structural convergence due to mechanistic constraints typically occurs in only those parts of a protein with clear mechanistic roles, such as the catalytic dyads and triads of enzymes. For example, a comprehensive survey of convergence in analogous enzymes identified 267 pairs with similar dyads or triads, but none with similar folds (Gherardini et al., 2007). Fold space is evidently large enough that many folds are likely to be compatible with a given mechanism.

Perhaps the most extensive known case of structural convergence in functionally similar helical IMPs occurred among thiol oxidoreductases. Four analogous families all use four-helix bundles to bind their redox cofactors, despite two being IMPs and two being cytoplasmic (Li et al., 2018). But they are nonetheless easily distinguishable because they connect those four helices in different orders. This indicates that even an exceptionally tight constraint on the architecture of secondary structure elements does not comparably constrain the connectivity of those elements. Indeed, the seven TMHs of another IMP, rhodopsin, can be experimentally permuted while retaining activity (Mackin et al., 2014). 36 such permutations are possible for proto-SecY H0-5. Although some permutations would be more likely to evolve than others, analogy is likelier than homology only if the observed connectivity is likelier than all 35 others combined. Thus even if the specific architectures of SecY and YidC were favoured by some yet unknown mechanistic constraint, their identical connectivity would still support the homology hypothesis.

Without functional or mechanistic constraints, structural convergence can still occur in some cases due to folding constraints imposed by the intrinsic properties of polypeptide and solvent. One would expect such intrinsically preferred structures to occur frequently and in functionally unrelated contexts. For this reason the phylogeny of ubiquitous and functionally diverse folds is challenging to discern (Lupas et al., 2001). But it is implausible that folding constraints strongly favour the SecY/Oxa1 fold because it is not found in other proteins, as our database queries show.

Finally, we consider the most detailed similarity between SecY and YidC, which is in their H5 sequence profiles. If H5 was in the same transmembrane position and orientation in both proteins, one might imagine that this sequence similarity was a product of mechanistic constraints. However, H5's sequence profile occurs despite topological inversion (Figure 6), and thus lends at least some weight to homology. Just how how much weight is unclear. Ideally one would compare SecY and

YidC to analogous proteins with the same structure and function and see how exceptional their sequence similarity is among that set. Such a test is partly feasible for proteins with very common folds, like β-barrels (Remmert et al., 2010), but impossible here, because our database queries find no other proteins with the SecY/Oxa1 fold.

In sum, the dispositive evidence for homology between SecY and the Oxa1 superfamily is structural. It would be empirically unprecedented and theoretically improbable for their structural similarity to arise by convergence. We therefore conclude that they are more likely to be homologs than analogs, and describe them as homologs hereafter.

## Implications for the evolution of protein transport

Besides illuminating SecY's origins, identifying YidC as its progenitor implies that YidC is the oldest known channel. This has implications for the evolution of IMPs generally, including YidC itself, and other ancient components of the general secretory pathway: SecEG (Cao and Saier, 2003; Kinch et al., 2002; Figure 11-Figure supplement 1), signal peptidase (Rawlings and Bateman, 2019), SRP and SRP receptor (SR; Gribaldo and Cammarano, 1998). We propose that the following stepwise model (Figure 11) is the simplest that is consistent with the available data.

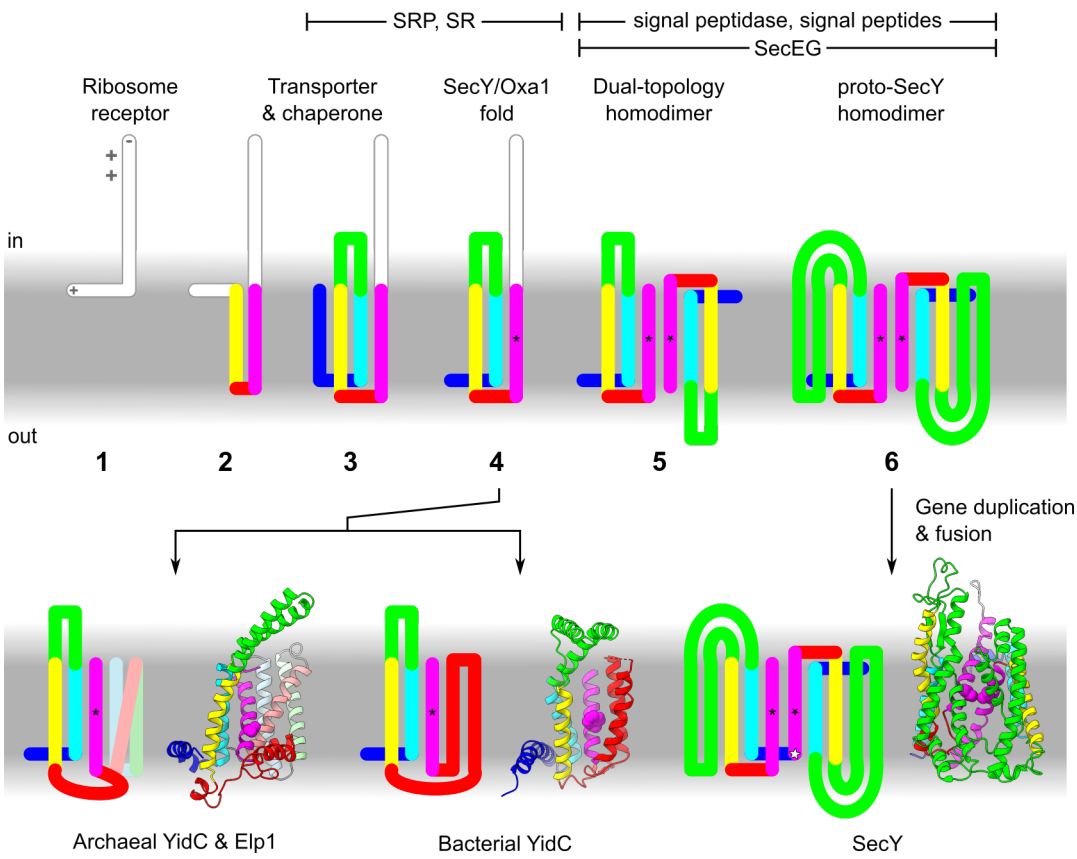


**Figure 11.** Model for the evolution of YidC and SecY. Charged side chains and termini are indicated only at stage 1, by grey symbols. Asterisks indicate the pore ring or groove end residue in H5. At top, additional components of the secretory pathway label a range of stages at which they they may have arisen. Models show archaeal YidC and Elp1 (*M. jannaschii* MJ0480 and MJ0606, trRosetta), bacterial YidC (*B. halodurans* YidC2, 3wo6), and SecY (*G. thermodenitrificans* SecY, 6itc).
**Figure 11-Figure supplement 1.** Similarity between archaeal and bacterial SecG.

Step 1. An ancestor of YidC was a membrane-peripheral ribosome receptor. This is parsimonious insofar as both YidC and SecY are ribosome receptors, and like all IMPs presumably descend from peripheral proteins (Mulkidjanian et al., 2009). Ribosome receptor function can be achieved with just two low-complexity domains: a weakly hydrophobic anchor and a polybasic extension. This receptor would reduce aggregation of hydrophobic domains in the aqueous phase by creating a population of membrane-bound ribosomes, from which any nascent IMPs would be more likely to encounter the membrane. Similar polybasic C-terminal tails are known to occur in YidC and can compensate for deletion of SRP or SR (Seitl et al., 2014; Szyrach et al., 2003).

Step 2. The peripheral helix acquires a transmembrane hairpin, thereby integrating into the membrane. Uncatalyzed insertion of a hairpin is more efficient than that of a single TMH (Engelman and Steitz, 1981), making a hairpin the more likely initial membrane anchor. We infer that SRP/SR-dependent targeting did not evolve until after this and other minimal IMPs existed for it to target. The proximity of this hairpin to nascent IMPs emerging from the bound ribosome imposes a selective pressure on the hairpin to evolve membrane-buried hydrophilic residues that can facilitate IMP integration. Substrates would engage this YidC ancestor in the same hairpin conformation that is favoured during uncatalysed translocation, and this conformation remains how substrates engage SecY and YidC today.

Step 3. Acquisition of a second transmembrane hairpin produces a four-TMH protein containing the conserved three-helix bundle and hydrophilic groove. The segment between the first and second transmembrane hairpins becomes the cytosolic hairpin H2/3. The additional TMHs allow YidC to form a hydrophilic groove in the membrane, thereby further facilitating substrate translocation.

Step 4. The hydrophilic groove allows hydrophilic termini to efficiently translocate, including the N-terminus of the YidC ancestor itself, which acquires a new position as the extracytoplasmic peripheral helix H0. Thus the full SecY/Oxa1 fold is now attained. By this time, SRP/SR have evolved, and H2/3 evolves interactions with SR and the ribosome, features that are still evident in SecY, YidC, and TMCO1 (Kuhn et al., 2011; McGilvray et al., 2020; Petriman et al., 2018). At this stage, the YidC gene duplicated, allowing one paralog to seed the SecY lineage. Paralogous origin in a tandem duplication event would be consistent with the commonly observed juxtaposition of YidC and SecY in prokaryotic genomes (Makarova et al., 2015).

Step 5. The original ribosome-binding tail is lost due to its redundancy with SRP/SR for targeting and H2/3 for docking. Loss of this element and genetic drift yields a subpopulation of inverted proteins. Antiparallel dimerisation of the two subpopulations would be favoured because the monomers prefer a similarly thinned membrane, especially near the distal face of H5. Hydrophobic interactions between the groove end residues would favour the particular dimer symmetry of SecY, which juxtaposes them. The non-SecY lineage of YidC (from step 4) evolves in archaea to heterodimerise with Elp1 via the distal face of H5; in bacteria, this same surface becomes covered by the h4h5 transmembrane hairpin.

Antiparallel homodimerisation in the SecY lineage positions hydrophilic grooves on both sides of the membrane, leaving at most a thin hydrophobic layer between them, as in the heterodimeric ERAD channel (Wu et al., 2020). This facilitates the translocation of IMPs with large soluble domains, including signal peptidase. In the presence of signal peptidase, signal-dependent secretion becomes possible, with the first cleavable signal peptides being the TMHs of IMPs

which had previously anchored their now-secreted extracytoplasmic domains. Signal peptides originating as TMHs would explain why both engage SecY in a similar way.

At this stage or later, SecEG are acquired. SecE's symmetrical binding to each half of the dimer would stabilise it, particularly when the monomers separate to accommodate substrates. In SecY, SecE remains the axis about which the N-half pivots during gating (Voorhees and Hegde, 2016). Evolution of SecEG after YidC but before proto-SecY would explain why their integration depends on other Oxa1 superfamily members and not SecY (Guna et al., 2018; Yi et al., 2003).

Step 6. Transmembrane insertion of H2/3 creates a lateral gate, and thus the proto-SecY fold. By inserting between the hydrophilic grooves and the membrane, H2/3 makes those grooves deeper and more hydrophilic, further facilitating translocation. As a secondary consequence, it also creates a more hydrophilic environment for signal recognition. This allows cleavable signal peptides to become less hydrophobic than TMHs, and thus more easily distinguished by signal peptidase.

Duplication and fusion of the proto-SecY gene would allow each half of this initially symmetric protein to specialise for cytoplasmic and extracytoplasmic functions. For example, the C.h1h2 and C.h4h5 loops would continue to bind ribosomes, whereas these same loops in the N-half atrophy. One such loop was repurposed as the plug. We infer that gene duplication occurred after antiparallel dimerisation because this has precedent (Lolkema et al., 2008; Rapp et al., 2006) and because both halves of SecY conserve the transmembrane insertion of H2/3, which appears to be an adaptation to antiparallel dimerisation.

## Outlook

One might hope that the increasing diversity of known IMP structures will reveal the origins of other pseudosymmetric channels, which have been refractory to sequence searches (Hennerdal et al., 2010). But the detectability of SecY's origins may be due to the unusual properties of protein as a transport substrate. Unlike most substrates, protein can be sufficiently hydrophobic to assist in its own translocation, making an incompletely penetrant channel such as YidC functionally sufficient. Moreover YidC is thought to serve a second function as a chaperone for IMP folding, which makes it non-redundant to SecY. The same hydrophilic groove used for transport is thought to mediate this chaperone function (Kumazaki et al., 2014; Nagamori et al., 2004; Serdiuk et al., 2016). Other pre-fusion channel precursors may have exposed similar grooves for transport, but this non-redundant chaperone function is unique to protein substrates. Thus pre-fusion homologs of other channels may have had less reason to be conserved.

Although theories about early evolutionary transitions are not experimentally testable, experimental reconstructions can at least demonstrate their plausibility. Efforts to reconstruct the earliest cells, called protocells, could capitalise on the synergy detailed above between YidC and the putative primordial protein-secreting translocase (Mulkidjanian et al., 2007). This protein translocase is itself thought to descend from an RNA translocase, in part because its ATPase domain descends from an RNA helicase. By facilitating the integration of such an RNA translocase, YidC would have indirectly facilitated the exchange of genetic information among protocells, thereby allowing recombination to continue despite cellularisation and accelerating this stage of evolution.

Since early studies on protein transport, it has been theorised that protocells were preceded by

inside-out precursors, called obcells, which arose when macromolecules colonised the surface of a vesicle (Blobel, 1980). The obcell's interior would then become the protocell's periplasm after an involution akin to gastrulation. The obcell stage would be the earliest that could have hosted protein transporters, but may have featured only a rudimentary genetic code (Cavalier-Smith, 2001). Consistent with such an early origin, the conserved pore and groove residues identified here (proline, glycine, serine, branched aliphatics) are all abiotically generated (Weber and Miller, 1981) and thought to be among the first encoded (Trifonov, 2000). Moreover even the simplest ancestors of YidC modelled here served functions that would be useful during the colonisation of a membrane. Thus this stage is a reasonable early bound for the origin of YidC. More precise estimates may require more detailed contextual knowledge about protocells and their precursors.

## Acknowledgements

A.J.O.L. is funded by the UK Medical Research Council and the Cambridge Commonwealth, European and International Trust. R.S.H is funded by the UK Medical Research Council (MC_UP_A022_1007). For critically reading the manuscript, we thank Robert J Keenan, John P O'Donnell, and Viswanathan Chandrasekaran.

## Methods

### Sequence similarity measures, datasets and queries

SecY sequence analyses used a recently published dataset of taxonomically diverse prokaryotic sequences (Harris and Goldman, 2021). To this dataset, we added the sequences for two structurally characterised SecY (*G. thermodenitrificans* and *M. jannaschii*) and removed 8 fully redundant sequences, 3 highly divergent Elusimicrobia sequences, and 4 N-terminally truncated sequences. The resulting alignment contains 342 sequences, 263 bacterial and 79 archaeal. Sequences were aligned with MAFFT L-INS-i. This and subsequent MAFFT alignments used default parameters, except for using the alternative gap extension penalty --ep 0.123 that is standard for sequences without domain-scale indels.

Pairwise sequence identities were calculated by re-alignment with ClustalOmega (Sievers and Higgins, 2021) on the European Bioinformatics Institute server (Madeira et al., 2019). Clustal reports an all-against-all identity matrix and has previously been used to quantify long-term evolutionary trends in sequence identity (Konaté et al., 2019). Default parameters were used. The number of pairwise comparisons was $342^2$ for the SecY halves, 89×75 for the ComEA and UvrC $(HhH)_2$ families, and 79×263 for archaeal and bacterial SecY. Sequences were shuffled to estimate excess identity using the Sequence Manipulation Suite (Stothard, 2000).

HHpred pairwise comparisons and database queries used the Max Planck Institute for Developmental Biology's server (Zimmermann et al., 2018). All used default parameters. The HHpred *p* between the full-length SecY halves was calculated using their subsequences from *M. jannaschii* SecY as input for automatic MSA generation. Database queries pertaining to EMC6/GET2 homologs used the *H. sapiens* EMC6 (NP_001014764.1), GET2 (NP_001736.1), or *Lokiarchaeum sp. GC14_75* Lokiarch_50810 (KKK40543.1) sequence.

The N- and C-half sequences were aligned using the structurally similar regions of H1-5 as a seed

alignment, to which the 684 N- and C-half sequences were added using MAFFT L-INS-i --seed. This alignment of halves was used as input to ConSurf (Ashkenazy et al., 2016) to score the conservation of each column across the two halves. Conservation scores for *B. halodurans* YidC2 were obtained from ConSurf-DB (Chorin et al., 2020).

Archaeal YidC sequences were collected from Pfam family PF01956. All UniProt sequences assigned to PF01956 were retrieved, and non-archaeal sequences (EMC3 and TMCO1) were excluded. To speed subsequent alignment, the archaeal sequences were filtered at 80% sequence identity using MMseqs2 (Steinegger and Söding, 2017), in target-coverage mode so as to preferentially eliminate fragments. The resulting 871 sequences were aligned by MAFFT L-INS-i.

### Structural similarity measures and database queries

Each SecY model was split into N- and C-halves at an arbitrary point in the poorly conserved loop between them close to the C-terminus of N.H5. The resulting half-SecY structures were multiply aligned and compared by TM-score using the Zhang group's mTM-align server (Dong et al., 2018a, 2018b), which also reports their number of common core a.a. and RMSD.

Dali queries against the PDB25 were performed using the Holm group's server (Holm, 2020). The Dali PDB25 is a subset filtered at 25% maximum pairwise sequence identity, and excludes some additional structures, including TMCO1 (6w6l), due to file format incompatibilities. It contained 21390 chains when queried. Results were manually reviewed to exclude hits with SecY family or regions that are not transmembrane. Dali *Z*-scores were equated to *p*-values by assuming an extreme value distribution of scores as in Sierk and Pearson, 2004,

$$p = 1 - \exp\left(-\exp\left(\frac{\pi}{\sqrt{6}} Z - \gamma\right)\right)$$

where $\gamma$ is Euler's constant.

### Co-evolutionary structure and contact prediction

Structural models were predicted from amino acid sequences using the trRosetta algorithm (Yang et al., 2020). End-to-end pipelines which automate the intermediate steps of multiple-sequence alignment generation and homology template selection were used, which reduces user input to only the single protein sequence of interest. The Baker lab's server (for Ylp1) and the Yang lab's server (for the EMC6 family) were used.

NCBI RefSeq accession numbers for the EMC6/GET2 homolog sequences used as queries are as follows: *P. horikoshii* WP_010885465.1, *Lokiarchaeum sp. GC14_75* KKK40543.1, *S. solfataricus* WP_009990433.1, *M. jannaschii* WP_010870110.1, *A. fulgidus* WP_010878056.1, *Methanosarcina* WP_011032380.1, *M. fervidus* WP_013413780.1, *T. acidophilum* WP_010900743.1, *H. jilantaiense* WP_089668789.1, *H. sapiens* NP_061328.1 (C20orf24 isoform a, a.k.a. UniParc isoform 2, Q9BUV8-2). For the sequences most similar to eukaryotic EMC6, yeast and human EMC6 were automatically selected as homology templates (PDB 6wb9, 6z3w), as indicated in Figure 8-Figure supplement 2a.

Heterodimeric contacts were predicted from amino acid sequences using the RaptorX ComplexContact algorithm (Zeng et al., 2018) as provided by the Xu group's web server. The

multiple-sequence alignments generated by RaptorX ComplexContact for MJ0606 and C20orf24 were reviewed to ensure that they did not include any proteins annotated as EMC6.

### Figure preparation

All models were aligned and rendered in UCSF ChimeraX (Pettersen et al., 2020). Surface hydrophobicity was computed in ChimeraX by its default method: pyMLP (Broto et al., 1984; Laguerre et al., 1997) with Fauchere propagation and lipophilicity values from Ghose et al., 1998. Models depicted relative to a membrane are positioned and oriented according to the prediction algorithm provided by the Orientations of Proteins in Membranes server (Lomize et al., 2012). OPM does not account for any anisotropy which lipid-exposed hydrophilic residues may induce, and thus none is shown. YidC's position was adjusted 1.8 Å toward the lumen to agree with molecular dynamics simulations in which a conserved arginine in H1 (homologous to *B. halodurans* YidC2 R72) sits at the bilayer midplane (Chen et al., 2017). The membrane's interfacial layers are shown as linear gradients half the width the hydrophobic layer, to approximate experimentally determined polarity profiles (White and Wimley, 1999).

Per-residue hydropathy and charge were computed from protein sequences using EMBOSS Pepinfo (Madeira et al., 2019), topology predicted using TMHMM (Krogh et al., 2001), and plotted in Veusz. The 2-D histogram of IMP length *vs* TMH count was likewise plotted in Veusz.

## Supplementary Note

We sought to estimate the amino acid sequences of cenancestral SecY and proto-SecY. A recent study of another internally duplicated cenancestral protein, the helix-hairpin-helix $(HhH)_2$, demonstrated that maximum likelihood (ML) tree inference using IQ-TREE (Trifinopoulos et al., 2016) and empirical Bayesian ancestral sequence reconstruction (ASR) could yield a cenancestral sequence with dramatically increased sequence identity between its duplicated domains (from 21 ± 8% to 46%; Longo et al., 2020). Here we apply similar methods to a recently published dataset of taxonomically diverse prokaryotic SecY sequences (Harris and Goldman, 2021). The published alignment of these sequences is inconsistent with a structural alignment around C.H1 (Supplementary figure 1), but aligning the sequences using MAFFT L-INS-i yields results consistent with the structures, so we use this realignment for our analysis. A few sequences were added to or removed to yield a final full-length (FL) alignment, as described in the Methods.

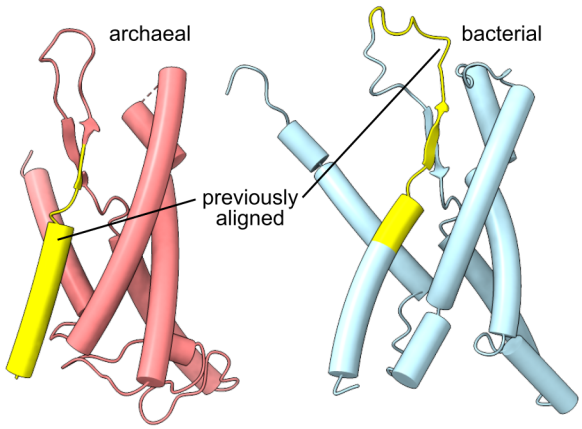


**Supplementary figure 1.** Discrepancy between a structural alignment of archaeal and bacterial C.H1 and the previous sequence alignment of Harris and Goldman, 2021. Archaeal (*M. jannaschii*, 1rh5) and bacterial SecY (*G. thermodenitrificans*, 6itc) C-halves are shown, with a previously sequence-aligned segment highlighted in yellow.

In addition to the FL alignment, we also prepared a structure-guided alignment of the N- and C-half subsequences from the same dataset, as described in the Methods, and used this NC alignment as a separate basis for ASR. Finally, we also used a version of the NC alignment which includes only the five structurally aligned blocks corresponding to H1-5 (NC-blocks).

Matched-pair tests (Naser-Khdour et al., 2019) did not reject the standard assumptions of symmetry and homogeneity ($p > 5\%$), although the data in NC-blocks were insufficient for most tests. Automated phylogenetic model selection was performed with ModelFinder (Kalyaanamoorthy et al., 2017) by the Bayesian information criterion (BIC). In each case, the same model would have been selected by the Akaike information criterion (AIC), whereas the corrected AIC (AICc), which more strongly avoids overfitting, would select a less parameter-rich model. Likelihood mapping (Strimmer and von Haeseler, 1997) showed that while the phylogenetic signal in all three alignments is poor, it is strongest in the FL alignment, and not much degraded by reducing NC to NC-blocks. ML tree inference with IQ-TREE 2 (Minh et al., 2020) was performed with 1000 ultrafast bootstrap replicates (Hoang et al., 2018).

| | FL | NC | NC-blocks |
|---|---|---|---|
| % gaps | 51 | 67 | 0 |
| **sites** | 914 | 678 | 102 |
| parsimony-informative | 630 | 423 | 102 |
| singleton | 118 | 104 | 0 |
| constant | 166 | 151 | 0 |
| **sequences** | 342 | 684 | 684 |
| composition $\chi^2$ test $p < 5\%$ | 9 | 10 | 2 |
| **matched pair test *p*** | | | |
| symmetry | 0.23 | 0.56 | 0.62 |
| marginal symmetry | 0.32 | 0.88 | n/a |
| internal symmetry | 0.26 | 0.34 | n/a |
| **model selection** | | | |
| BIC | LG+F+R9 | LG+F+R10 | Q.yeast+F+R9 |
| AIC | LG+F+R9 | LG+F+R10 | Q.yeast+F+R9 |
| AICc | LG+F+R8 | LG+G4 | LG |
| **likelihood mapping** | | | |
| % fully resolved | 66 | 55 | 52 |
| % partially resolved | 22 | 3 | 3 |
| % unresolved | 12 | 42 | 45 |
| total tree length | 313 | 147 | 163 |

**Supplementary table 1.** Summary statistics from sequence alignment and phylogenetic inference. Abbreviations: LG, Le & Gascuel substitution matrix (Le and Gascuel, 2008); F, empirical amino acid frequencies; R, rate categories; G, gamma-distributed rate categories; Q.yeast, QMaker yeast-specific substitution matrix (Minh et al., 2021).

The FL tree accurately reflects most of the shallow relationships within phyla, as in Harris & Goldman 2021. But the deepest branch, between archaea and bacteria, is extraordinarily long, 5.9 expected substitutions per site (sps), which means the overwhelming majority of sites should be expected to differ in both archaea and bacteria from whatever their identity was in the cenancestor (Supplementary figure 2a). This length may be regarded as a lower bound on the true branch length, since excluding the fastest-evolving sites or using more parameter-rich models typically yields even longer archaeal-bacterial branches (Moody et al., 2021). It is thus unsurprising that ancestral sequences reconstructed at the root nodes of archaea or bacteria, using IQ-TREE 2's implementation of the empirical Bayesian method, displayed halves with poor sequence similarity (15-20% identity across H1-5), not significantly different from that between the halves of extant sequences (16 ± 3% across H1-5).

The NC and NC-blocks alignments yielded trees with a long central branch separating the N-halves and C-halves (5.8, 6.8 sps; Supplementary figure 2b,c). The subtree for each of the two halves displayed some topological discrepancies with the other half's subtree. These discrepancies were particularly acute in the NC-blocks tree, which puts the root of the N-half inside archaea, but the root of the C-half inside bacteria. Such extreme discrepancies are common in trees of universal paralogs, which are generally so divergent that outgroup rooting is inadvisable due to severe model violations (Gouy et al., 2015).

Unlike the NC-blocks tree, the NC tree places the root of both subtrees between archaea and bacteria. This difference is difficult to attribute to any meaningful signal in the data, since the NC-blocks alignment retains the high-confidence columns from structural alignment and nearly as much phylogenetic signal as the NC alignment (Supplementary table 1). It may instead be an artefact of

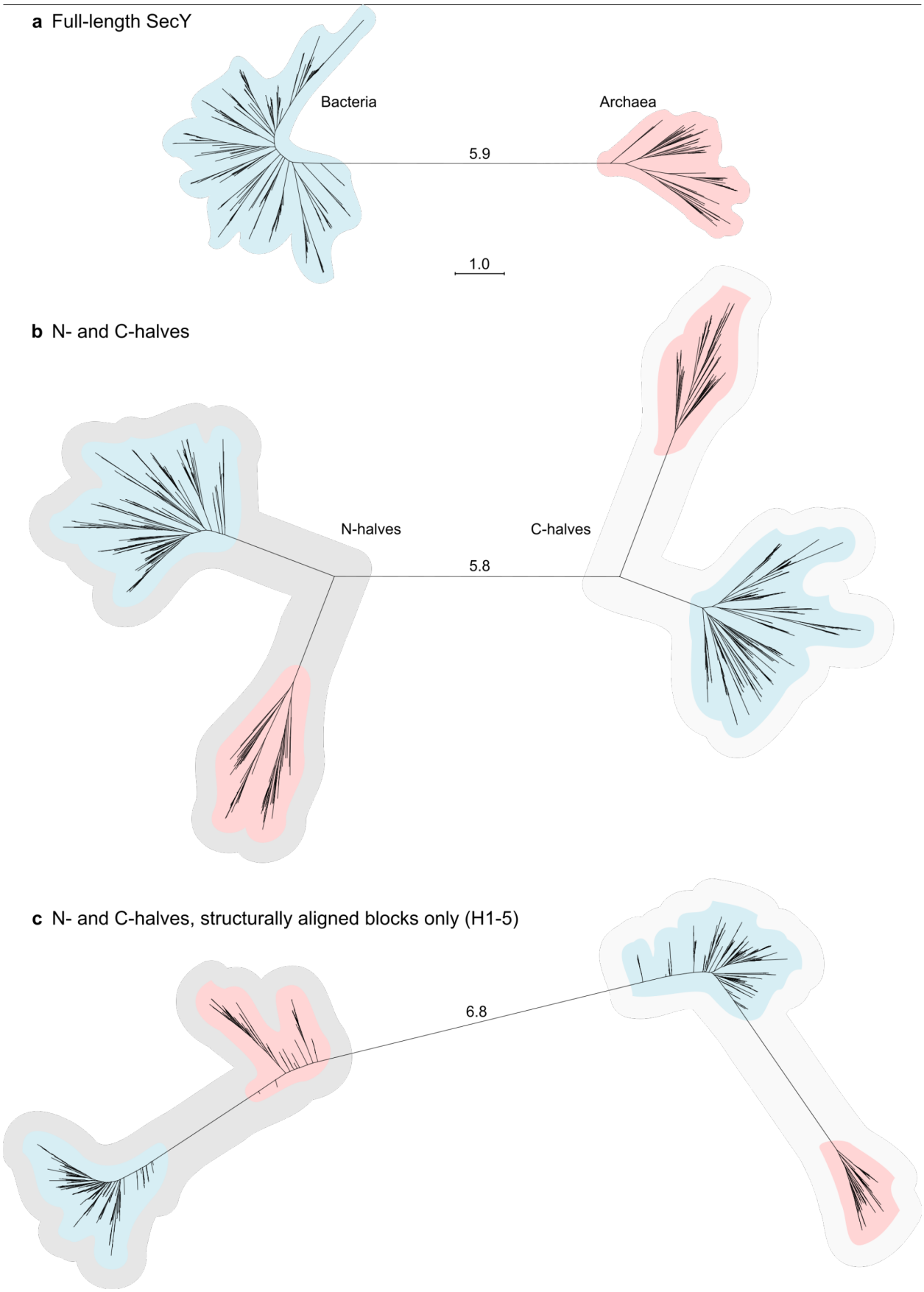


**Supplementary figure 2.** Maximum likelihood trees inferred for SecY and its halves. All trees are shown on the same scale. The length unit is the expected number of substitutions per site. **a** Tree inferred from the FL alignment. **b** Tree inferred from the NC alignment. **c** Tree inferred from the NC-blocks alignment.

long branch attraction (LBA), induced by the greater number of high variability and poorly aligned sites contained in the NC alignment. The indistinguishability of this tree topology from what LBA would induce makes the accuracy of universal paralog trees suspect in general (Gouy et al., 2015). Thus although one could estimate ancestral N- and C-half and proto-SecY sequences using these

The methods applied here may have proven less effective than when previously applied to HhH domains (Longo et al., 2020) because those domains are less divergent than the SecY halves. The HhH domains each conserve independent nucleotide-binding activity, and thus are just as conserved as are the $(HhH)_2$ proteins as a whole (22.4 ± 7.8% between domains *vs* 19.5 ± 4.4% between UvrC and ComEA). By contrast, the SecY domains form an obligate complex around a single active site, and are much less conserved than SecY as a whole (12.5 ± 2.2% between domains *vs* 20.3 ± 1.6% between archaea and bacteria). It is also known that general-purpose substitution models like LG, used here, are a poor fit to substitutions occurring in the heterogeneous membrane environment (Jones et al., 1994). Regardless of the true cause, the sequences of SecY's ancestors remain recondite. The main text therefore focuses on more stable characteristics, namely structure, mechanism, function, and a few functionally important, highly conserved residues.

## References


Andersson, H., and von Heijne, G. (1993). Sec dependent and sec independent assembly of E. coli inner membrane proteins: the topological rules depend on chain length. The EMBO Journal *12*, 683–691.

Anghel, S.A., McGilvray, P.T., Hegde, R.S., and Keenan, R.J. (2017). Identification of Oxa1 homologs operating in the eukaryotic endoplasmic reticulum. Cell Reports *21*, 3708–3716.

Ashkenazy, H., Abadi, S., Martz, E., Chay, O., Mayrose, I., Pupko, T., and Ben-Tal, N. (2016). ConSurf 2016: an improved methodology to estimate and visualize evolutionary conservation in macromolecules. Nucleic Acids Research *44*, W344–W350.

Bai, L., You, Q., Feng, X., Kovach, A., and Li, H. (2020). Structure of the ER membrane complex, a transmembrane-domain insertase. Nature *584*, 475–478.

Bakelar, J., Buchanan, S.K., and Noinaj, N. (2016). The structure of the β-barrel assembly machinery complex. Science *351*, 180–186.

Bauer, M., Behrens, M., Esser, K., Michaelis, G., and Pratje, E. (1994). PET1402, a nuclear gene required for proteolytic processing of cytochrome oxidase subunit 2 in yeast. Molec. Gen. Genet. *245*, 272–278.

Beltzer, J.P., Fiedler, K., Fuhrer, C., Geffen, I., Handschin, C., Wessels, H.P., and Spiess, M. (1991). Charged residues are major determinants of the transmembrane orientation of a signal-anchor sequence. J. Biol. Chem. *266*, 973–978.

Blobel, G. (1980). Intracellular protein topogenesis. PNAS *77*, 1496–1500.

Bonnefoy, N., Chalvet, F., Hamel, P., Slonimski, P.P., and Dujardin, G. (1994). OXA1, a Saccharomyces cerevisiae Nuclear Gene whose Sequence is Conserved form Prokaryotes to Eukaryotes Controls Cytochrome Oxidase Biogenesis. Journal of Molecular Biology *239*, 201–212.

Borowska, M.T., Dominik, P.K., Anghel, S.A., Kossiakoff, A.A., and Keenan, R.J. (2015). A YidC-like Protein in the Archaeal Plasma Membrane. Structure *23*, 1715–1724.

Bowie, J.U. (1997). Helix packing in membrane proteins11Edited by G. von Heijne. Journal of Molecular Biology *272*, 780–789.

Braunger, K., Pfeffer, S., Shrimal, S., Gilmore, R., Berninghausen, O., Mandon, E.C., Becker, T., Förster, F., and Beckmann, R. (2018). Structural basis for coupling protein transport and N-glycosylation at the mammalian endoplasmic reticulum. Science *360*, 215–219.

BROTO, P., MOREAU, G., and VANDYCKE, C. (1984). Molecular structures: perception, autocorrelation descriptor and sar studies: system of atomic contributions for the calculation of the n-octanol/water partition coefficients. Eur. j. Med. Chem *19*, 71–78.

Brown, J., Behnam, R., Coddington, L., Tervo, D.G.R., Martin, K., Proskurin, M., Kuleshova, E., Park, J., Phillips, J., Bergs, A.C.F., et al. (2018). Expanding the Optogenetics Toolkit by Topological Inversion of Rhodopsins. Cell *175*, 1131-1140.e11.

Brunner, J.D., Lim, N.K., Schenck, S., Duerst, A., and Dutzler, R. (2014). X-ray structure of a calcium-activated TMEM16 lipid scramblase. Nature *516*, 207–212.

Cao, T.B., and Saier, M.H. (2003). The general protein secretory pathway: phylogenetic analyses leading to evolutionary conclusions. Biochimica et Biophysica Acta (BBA) - Biomembranes *1609*, 115–125.

Cavalier-Smith, T. (2001). Obcells as Proto-Organisms: Membrane Heredity, Lithophosphorylation, and the Origins of the Genetic Code, the First Cells, and Photosynthesis. Journal of Molecular Evolution *53*, 555–595.

Chen, Y., Capponi, S., Zhu, L., Gellenbeck, P., Freites, J.A., White, S.H., and Dalbey, R.E. (2017). YidC Insertase of Escherichia coli: Water Accessibility and Membrane Shaping. Structure *25*, 1403-1414.e3.

Chorin, A.B., Masrati, G., Kessel, A., Narunsky, A., Sprinzak, J., Lahav, S., Ashkenazy, H., and Ben-Tal, N. (2020). ConSurf-DB: An accessible repository for the evolutionary conservation patterns of the majority of PDB proteins. Protein Science *29*, 258–267.

Coleman, G.A., Davín, A.A., Mahendrarajah, T.A., Szánthó, L.L., Spang, A., Hugenholtz, P., Szöllősi, G.J., and Williams, T.A. (2021). A rooted phylogeny resolves early bacterial evolution. Science *372*.

Dalal, K., and Duong, F. (2009). The SecY complex forms a channel capable of ionic discrimination. EMBO Reports *10*, 762–768.

Dong, R., Pan, S., Peng, Z., Zhang, Y., and Yang, J. (2018a). mTM-align: a server for fast protein structure database search and multiple protein structure alignment. Nucleic Acids Research *46*, W380–W386.

Dong, R., Peng, Z., Zhang, Y., and Yang, J. (2018b). mTM-align: an algorithm for fast and accurate multiple protein structure alignment. Bioinformatics *34*, 1719–1725.

Doolittle, R.F. (1994). Convergent evolution: the need to be explicit. Trends in Biochemical Sciences *19*, 15–18.

Engelman, D.M., and Steitz, T.A. (1981). The spontaneous insertion of proteins into and across membranes: the helical hairpin hypothesis. Cell *23*, 411–422.

Erlandson, K.J., Miller, S.B.M., Nam, Y., Osborne, A.R., Zimmer, J., and Rapoport, T.A. (2008). A role for the two-helix finger of the SecA ATPase in protein translocation. Nature *455*, 984–987.

Esser, L., Zhou, F., Yu, C.-A., and Xia, D. (2019). Crystal structure of bacterial cytochrome bc1 in complex with azoxystrobin reveals a conformational switch of the Rieske iron–sulfur protein subunit. J. Biol. Chem. *294*, 12007–12019.

Forrest, L.R. (2015). Structural Symmetry in Membrane Proteins. Annual Review of Biophysics *44*, 311–337.

Gherardini, P.F., Wass, M.N., Helmer-Citterich, M., and Sternberg, M.J.E. (2007). Convergent Evolution of Enzyme Active Sites Is not a Rare Phenomenon. Journal of Molecular Biology *372*, 817–845.

Ghose, A.K., Viswanadhan, V.N., and Wendoloski, J.J. (1998). Prediction of

Hydrophobic (Lipophilic) Properties of Small Organic Molecules Using Fragmental Methods: An Analysis of ALOGP and CLOGP Methods. J. Phys. Chem. A *102*, 3762–3772.
Gimpelev, M., Forrest, L.R., Murray, D., and Honig, B. (2004). Helical Packing Patterns in Membrane and Soluble Proteins. Biophysical Journal *87*, 4075–4086.
Gogala, M., Becker, T., Beatrix, B., Armache, J.-P., Barrio-Garcia, C., Berninghausen, O., and Beckmann, R. (2014). Structures of the Sec61 complex engaged in nascent peptide translocation or membrane insertion. Nature *506*, 107–110.
Gouy, R., Baurain, D., and Philippe, H. (2015). Rooting the tree of life: the phylogenetic jury is still out. Philosophical Transactions of the Royal Society B: Biological Sciences *370*, 20140329.
Gribaldo, S., and Cammarano, P. (1998). The root of the universal tree of life inferred from anciently duplicated genes encoding components of the protein-targeting machinery. J Mol Evol *47*, 508–516.
Guna, A., and Hegde, R.S. (2018). Transmembrane domain recognition during membrane protein biogenesis and quality control. Current Biology *28*, R498–R511.
Guna, A., Volkmar, N., Christianson, J.C., and Hegde, R.S. (2018). The ER membrane protein complex is a transmembrane domain insertase. Science *359*, 470–473.
Guo, H., Suzuki, T., and Rubinstein, J.L. (2019). Structure of a bacterial ATP synthase. ELife *8*, e43128.
Gutiérrez-Fernández, J., Kaszuba, K., Minhas, G.S., Baradaran, R., Tambalo, M., Gallagher, D.T., and Sazanov, L.A. (2020). Key role of quinone in the mechanism of respiratory complex I. Nature Communications *11*, 4135.
Harris, A.J., and Goldman, A.D. (2021). The very early evolution of protein translocation across membranes. PLoS Computational Biology *17*, e1008623.
He, H., Kuhn, A., and Dalbey, R.E. (2020). Tracking the Stepwise Movement of a Membrane-inserting Protein In Vivo. Journal of Molecular Biology *432*, 484–496.
von Heijne, G. (1985). Signal sequences: The limits of variation. Journal of Molecular Biology *184*, 99–105.
Hell, K., Neupert, W., and Stuart, R.A. (2001). Oxa1p acts as a general membrane insertion machinery for proteins encoded by mitochondrial DNA. The EMBO Journal *20*, 1281–1288.
Hennerdal, A., Falk, J., Lindahl, E., and Elofsson, A. (2010). Internal duplications in α-helical membrane protein topologies are common but the nonduplicated forms are rare. Protein Science *19*, 2305–2318.
Hessa, T., Meindl-Beinker, N.M., Bernsel, A., Kim, H., Sato, Y., Lerch-Bader, M., Nilsson, I., White, S.H., and von Heijne, G. (2007). Molecular code for transmembrane-helix recognition by the Sec61 translocon. Nature *450*, 1026–1030.
Hoang, D.T., Chernomor, O., von Haeseler, A., Minh, B.Q., and Vinh, L.S. (2018). UFBoot2: Improving the Ultrafast Bootstrap Approximation. Molecular Biology and Evolution *35*, 518–522.
Holm, L. (2020). DALI and the persistence of protein shape. Protein Science *29*, 128–140.
Itskanov, S., Kuo, K.M., Gumbart, J.C., and Park, E. (2021). Stepwise gating of the Sec61 protein-conducting channel by Sec63 and Sec62. Nat Struct Mol Biol *28*, 162–172.
Janouškovec, J., Tikhonenkov, D.V., Burki, F., Howe, A.T., Rohwer, F.L., Mylnikov, A.P., and Keeling, P.J. (2017). A New Lineage of Eukaryotes Illuminates Early Mitochondrial Genome Reduction. Current Biology *27*, 3717-3724.e5.
Jones, D.T., Taylor, W.R., and Thornton, J.M. (1994). A mutation data matrix for transmembrane proteins. FEBS Letters *339*, 269–275.
Jonikas, M.C., Collins, S.R., Denic, V., Oh, E., Quan, E.M., Schmid, V., Weibezahn, J., Schwappach, B., Walter, P., Weissman, J.S., et al. (2009). Comprehensive Characterization of Genes Required for Protein Folding in the Endoplasmic Reticulum. Science *323*, 1693–1697.
Jungnickel, B., and Rapoport, T.A. (1995). A posttargeting signal sequence recognition event in the endoplasmic reticulum membrane. Cell *82*, 261–270.
Junne, T., Schwede, T., Goder, V., and Spiess, M. (2006). The plug domain of yeast Sec61p is important for efficient protein translocation, but is not essential for cell viability. Molecular Biology of the Cell *17*, 4063–4068.
Kalyaanamoorthy, S., Minh, B.Q., Wong, T.K.F., von Haeseler, A., and Jermiin, L.S. (2017). ModelFinder: fast model selection for accurate phylogenetic estimates. Nat Methods *14*, 587–589.
Kater, L., Frieg, B., Berninghausen, O., Gohlke, H., Beckmann, R., and Kedrov, A. (2019). Partially inserted nascent chain unzips the lateral gate of the Sec translocon. EMBO Reports *20*, e48191.
Kinch, L.N., Saier, J., Milton H., and Grishin, N.V. (2002). Sec61β – a component of the archaeal protein secretory system. Trends in Biochemical Sciences *27*, 170–171.
Konaté, M.M., Plata, G., Park, J., Usmanova, D.R., Wang, H., and Vitkup, D. (2019). Molecular function limits divergent protein evolution on planetary timescales. Elife *8*, e39705.
Krogh, A., Larsson, B., von Heijne, G., and Sonnhammer, E.L.L. (2001). Predicting transmembrane protein topology with a hidden markov model: application to complete genomes11Edited by F. Cohen. Journal of Molecular Biology *305*, 567–580.
Kuhn, A. (1988). Alterations in the extracellular domain of M13 procoat protein make its membrane insertion dependent on secA and secY. European Journal of Biochemistry *177*, 267–271.
Kuhn, P., Weiche, B., Sturm, L., Sommer, E., Drepper, F., Warscheid, B., Sourjik, V., and Koch, H.-G. (2011). The Bacterial SRP Receptor, SecA and the Ribosome Use Overlapping Binding Sites on the SecY Translocon. Traffic *12*, 563–578.
Kumazaki, K., Chiba, S., Takemoto, M., Furukawa, A., Nishiyama, K., Sugano, Y., Mori, T., Dohmae, N., Hirata, K., Nakada-Nakura, Y., et al. (2014). Structural basis of Sec-independent membrane protein insertion by YidC. Nature *509*, 516–520.
Laguerre, M., Saux, M., Dubost, J.P., and Carpy, A. (1997). MLPP: A Program for the Calculation of Molecular Lipophilicity Potential in Proteins. Pharmacy and Pharmacology Communications *3*, 217–222.
Lane, N., and Martin, W.F. (2012). The Origin of Membrane Bioenergetics. Cell *151*, 1406–1416.
Le, S.Q., and Gascuel, O. (2008). An improved general amino acid replacement matrix. Molecular Biology and Evolution *25*, 1307–1320.
Li, L., Park, E., Ling, J., Ingram, J., Ploegh, H., and Rapoport, T.A. (2016). Crystal structure of a substrate-engaged SecY protein-translocation channel. Nature *531*, 395.
Li, S., Shen, G., and Li, W. (2018). Intramembrane Thiol Oxidoreductases: Evolutionary Convergence and Structural Controversy. Biochemistry *57*, 258–266.
Li, W., Schulman, S., Boyd, D., Erlandson, K., Beckwith, J., and Rapoport, T.A. (2007). The Plug Domain of the SecY Protein Stabilizes the Closed State of the Translocation Channel and Maintains a Membrane Seal. Molecular Cell *26*, 511–521.
Lolkema, J.S., Dobrowolski, A., and Slotboom, D.-J. (2008). Evolution of Antiparallel Two-domain Membrane Proteins: Tracing Multiple Gene Duplication Events in the DUF606 Family. Journal of Molecular Biology *378*, 596–606.
Lomize, M.A., Pogozheva, I.D., Joo, H., Mosberg, H.I., and Lomize, A.L. (2012). OPM database and PPM web server: resources for positioning of proteins in membranes. Nucleic Acids Research *40*, D370–D376.
Longo, L.M., Despotović, D., Weil-Ktorza, O., Walker, M.J., Jabłońska, J., Fridmann-Sirkis, Y., Varani, G., Metanis, N., and Tawfik, D.S. (2020). Primordial emergence of a nucleic acid-binding protein via phase separation and statistical ornithine-to-arginine conversion. PNAS *117*, 15731–15739.
Lupas, A.N., Ponting, C.P., and Russell, R.B. (2001). On the Evolution of Protein Folds: Are Similar Motifs in Different Protein Folds the Result of Convergence, Insertion, or Relics of an Ancient Peptide World? Journal of Structural Biology *134*, 191–203.
Ma, C., Wu, X., Sun, D., Park, E., Catipovic, M.A., Rapoport, T.A., Gao, N., and Li, L. (2019). Structure of the substrate-engaged SecA-SecY protein translocation machine. Nature Communications *10*, 2872.
Mackin, K.A., Roy, R.A., and Theobald, D.L. (2014). An Empirical Test of Convergent Evolution in Rhodopsins. Molecular Biology and Evolution *31*, 85–95.
Madeira, F., Park, Y. mi, Lee, J., Buso, N., Gur, T., Madhusoodanan, N., Basutkar, P., Tivey, A.R.N., Potter, S.C., Finn, R.D., et al. (2019). The EMBL-EBI search and sequence analysis tools APIs in 2019. Nucleic Acids Research *47*, W636–W641.
Makarova, K.S., Galperin, M.Y., and Koonin, E.V. (2015). Comparative genomic analysis of evolutionarily conserved but functionally uncharacterized membrane proteins in archaea: Prediction of novel components of secretion, membrane remodeling and glycosylation systems. Biochimie *118*, 302–312.
Mariappan, M., Mateja, A., Dobosz, M., Bove, E., Hegde, R.S., and Keenan, R.J. (2011). The mechanism of membrane-associated steps in tail-anchored protein insertion. Nature *477*, 61.
Matlack, K.E., Mothes, W., and Rapoport, T.A. (1998). Protein translocation: tunnel vision. Cell *92*, 381–390.
McDowell, M.A., Heimes, M., Fiorentino, F., Mehmood, S., Farkas, Á., Coy-Vergara, J., Wu, D., Bolla, J.R., Schmid, V., Heinze, R., et al. (2020). Structural Basis of Tail-Anchored Membrane Protein Biogenesis by the GET Insertase Complex. Molecular Cell.
McGilvray, P.T., Anghel, S.A., Sundaram, A., Zhong, F., Trnka, M.J., Fuller, J.R., Hu, H., Burlingame, A.L., and Keenan, R.J. (2020). An ER

translocon for multi-pass membrane protein biogenesis. ELife *9*, e56889.
McKenna, M.J., Sim, S.I., Ordureau, A., Wei, L., Harper, J.W., Shao, S., and Park, E. (2020). The endoplasmic reticulum P5A-ATPase is a transmembrane helix dislocase. Science *369*.
Miller-Vedam, L.E., Bräuning, B., Popova, K.D., Schirle Oakdale, N.T., Bonnar, J.L., Prabu, J.R., Boydston, E.A., Sevillano, N., Shurtleff, M.J., Stroud, R.M., et al. (2020). Structural and mechanistic basis of the EMC-dependent biogenesis of distinct transmembrane clients. ELife *9*, e62611.
Minh, B.Q., Schmidt, H.A., Chernomor, O., Schrempf, D., Woodhams, M.D., von Haeseler, A., and Lanfear, R. (2020). IQ-TREE 2: New Models and Efficient Methods for Phylogenetic Inference in the Genomic Era. Molecular Biology and Evolution *37*, 1530–1534.
Minh, B.Q., Dang, C.C., Vinh, L.S., and Lanfear, R. (2021). QMaker: Fast and accurate method to estimate empirical models of protein evolution. Systematic Biology.
Moody, E.R.R., Mahendrarajah, T.A., Dombrowski, N., Clark, J.W., Petitjean, C., Offre, P., Szollosi, G.J., Spang, A., and Williams, T.A. (2021). Universal markers support a long inter-domain branch between Archaea and Bacteria. BioRxiv 2021.01.19.427276.
Mothes, W., Prehn, S., and Rapoport, T.A. (1994). Systematic probing of the environment of a translocating secretory protein during translocation through the ER membrane. EMBO J *13*, 3973–3982.
Mulkidjanian, A.Y., Makarova, K.S., Galperin, M.Y., and Koonin, E.V. (2007). Inventing the dynamo machine: the evolution of the F-type and V-type ATPases. Nature Reviews Microbiology *5*, 892–899.
Mulkidjanian, A.Y., Galperin, M.Y., and Koonin, E.V. (2009). Co-evolution of primordial membranes and membrane proteins. Trends in Biochemical Sciences *34*, 206–215.
Nagamori, S., Smirnova, I.N., and Kaback, H.R. (2004). Role of YidC in folding of polytopic membrane proteins. Journal of Cell Biology *165*, 53–62.
Naser-Khdour, S., Minh, B.Q., Zhang, W., Stone, E.A., and Lanfear, R. (2019). The Prevalence and Impact of Model Violations in Phylogenetic Analysis. Genome Biology and Evolution *11*, 3341–3352.
O'Donnell, J.P., Phillips, B.P., Yagita, Y., Juszkiewicz, S., Wagner, A., Malinverni, D., Keenan, R.J., Miller, E.A., and Hegde, R.S. (2020). The architecture of EMC reveals a path for membrane protein insertion. ELife *9*, e57887.
Ooi, C.E., and Weiss, J. (1992). Bidirectional movement of a nascent polypeptide across microsomal membranes reveals requirements for vectorial translocation of proteins. Cell *71*, 87–96.
Paetzel, M., Karla, A., Strynadka, N.C.J., and Dalbey, R.E. (2002). Signal peptidases. Chem Rev *102*, 4549–4580.
Park, E., and Rapoport, T.A. (2011). Preserving the membrane barrier for small molecules during bacterial protein translocation. Nature *473*, 239–242.
Park, E., and Rapoport, T.A. (2012). Mechanisms of Sec61/SecY-mediated protein translocation across membranes. Annual Review of Biophysics *41*, 21–40.
Park, E., Ménétret, J.-F., Gumbart, J.C., Ludtke, S.J., Li, W., Whynot, A., Rapoport, T.A., and Akey, C.W. (2014). Structure of the SecY channel during initiation of protein translocation. Nature *506*, 102–106.
Peltier, J.-B., Emanuelsson, O., Kalume, D.E., Ytterberg, J., Friso, G., Rudella, A., Liberles, D.A., Söderberg, L., Roepstorff, P., Heijne, G. von, et al. (2002). Central Functions of the Lumenal and Peripheral Thylakoid Proteome of Arabidopsis Determined by Experimentation and Genome-Wide Prediction. The Plant Cell *14*, 211–236.
Petersen, T.N., Brunak, S., von Heijne, G., and Nielsen, H. (2011). SignalP 4.0: discriminating signal peptides from transmembrane regions. Nature Methods *8*, 785–786.
Petriman, N.-A., Jauß, B., Hufnagel, A., Franz, L., Sachelaru, I., Drepper, F., Warscheid, B., and Koch, H.-G. (2018). The interaction network of the YidC insertase with the SecYEG translocon, SRP and the SRP receptor FtsY. Scientific Reports *8*, 578.
Petrov, A.S., Bernier, C.R., Hsiao, C., Norris, A.M., Kovacs, N.A., Waterbury, C.C., Stepanov, V.G., Harvey, S.C., Fox, G.E., Wartell, R.M., et al. (2014). Evolution of the ribosome at atomic resolution. PNAS *111*, 10251–10256.
Pettersen, E.F., Goddard, T.D., Huang, C.C., Meng, E.C., Couch, G.S., Croll, T.I., Morris, J.H., and Ferrin, T.E. (2020). UCSF ChimeraX: Structure visualization for researchers, educators, and developers. Protein Sci.
Plath, K., Mothes, W., Wilkinson, B.M., Stirling, C.J., and Rapoport, T.A. (1998). Signal Sequence Recognition in Posttranslational Protein Transport across the Yeast ER Membrane. Cell *94*, 795–807.
Pleiner, T., Tomaleri, G.P., Januszyk, K., Inglis, A.J., Hazu, M., and Voorhees, R.M. (2020). Structural basis for membrane insertion by the human ER membrane protein complex. Science *369*, 433–436.
Rapp, M., Granseth, E., Seppälä, S., and von Heijne, G. (2006). Identification and evolution of dual-topology membrane proteins. Nature Structural & Molecular Biology *13*, 112–116.
Rapp, M., Seppälä, S., Granseth, E., and Heijne, G. von (2007). Emulating Membrane Protein Evolution by Rational Design. Science *315*, 1282–1284.
Rawlings, N.D., and Bateman, A. (2019). Origins of peptidases. Biochimie *166*, 4–18.
Remmert, M., Biegert, A., Linke, D., Lupas, A.N., and Söding, J. (2010). Evolution of Outer Membrane β-Barrels from an Ancestral ββ Hairpin. Molecular Biology and Evolution *27*, 1348–1358.
Remmert, M., Biegert, A., Hauser, A., and Söding, J. (2012). HHblits: lightning-fast iterative protein sequence searching by HMM-HMM alignment. Nat Methods *9*, 173–175.
Rollauer, S.E., Tarry, M.J., Graham, J.E., Jääskeläinen, M., Jäger, F., Johnson, S., Krehenbrink, M., Liu, S.-M., Lukey, M.J., Marcoux, J., et al. (2012). Structure of the TatC core of the twin-arginine protein transport system. Nature *492*, 210–214.
Sääf, A., Johansson, M., Wallin, E., and Heijne, G. von (1999). Divergent evolution of membrane protein topology: The Escherichia coli RnfA and RnfE homologues. PNAS *96*, 8540–8544.
Samuelson, J.C., Chen, M., Jiang, F., Möller, I., Wiedmann, M., Kuhn, A., Phillips, G.J., and Dalbey, R.E. (2000). YidC mediates membrane protein insertion in bacteria. Nature *406*, 637–641.
Saracco, S.A., and Fox, T.D. (2002). Cox18p Is Required for Export of the Mitochondrially Encoded Saccharomyces cerevisiae Cox2p C-Tail and Interacts with Pnt1p and Mss2p in the Inner Membrane. MBoC *13*, 1122–1131.
Schmidt, A., Kochanowski, K., Vedelaar, S., Ahrné, E., Volkmer, B., Callipo, L., Knoops, K., Bauer, M., Aebersold, R., and Heinemann, M. (2016). The quantitative and condition-dependent Escherichia coli proteome. Nat Biotechnol *34*, 104–110.
Seitl, I., Wickles, S., Beckmann, R., Kuhn, A., and Kiefer, D. (2014). The C-terminal regions of YidC from Rhodopirellula baltica and Oceanicaulis alexandrii bind to ribosomes and partially substitute for SRP receptor function in Escherichia coli. Molecular Microbiology *91*, 408–421.
Serdiuk, T., Balasubramaniam, D., Sugihara, J., Mari, S.A., Kaback, H.R., and Müller, D.J. (2016). YidC assists the stepwise and stochastic folding of membrane proteins. Nature Chemical Biology *12*, 911–917.
Serdiuk, T., Steudle, A., Mari, S.A., Manioglu, S., Kaback, H.R., Kuhn, A., and Müller, D.J. (2019). Insertion and folding pathways of single membrane proteins guided by translocases and insertases. Science Advances *5*, eaau6824.
Shanmugam, S.K., Backes, N., Chen, Y., Belardo, A., Phillips, G.J., and Dalbey, R.E. (2019). New Insights into Amino-Terminal Translocation as Revealed by the Use of YidC and Sec Depletion Strains. Journal of Molecular Biology *431*, 1025–1037.
Shaw, A.S., Rottier, P.J., and Rose, J.K. (1988). Evidence for the loop model of signal-sequence insertion into the endoplasmic reticulum. Proc Natl Acad Sci U S A *85*, 7592–7596.
Sierk, M.L., and Pearson, W.R. (2004). Sensitivity and selectivity in protein structure comparison. Protein Science *13*, 773–785.
Sievers, F., and Higgins, D.G. (2021). The Clustal Omega Multiple Alignment Package. In Multiple Sequence Alignment, (Springer), pp. 3–16.
Söding, J. (2005). Protein homology detection by HMM–HMM comparison. Bioinformatics *21*, 951–960.
Stefer, S., Reitz, S., Wang, F., Wild, K., Pang, Y.-Y., Schwarz, D., Bomke, J., Hein, C., Löhr, F., Bernhard, F., et al. (2011). Structural Basis for Tail-Anchored Membrane Protein Biogenesis by the Get3-Receptor Complex. Science *333*, 758–762.
Steinegger, M., and Söding, J. (2017). MMseqs2 enables sensitive protein sequence searching for the analysis of massive data sets. Nature Biotechnology *35*, 1026–1028.
Stothard, P. (2000). The Sequence Manipulation Suite: JavaScript Programs for Analyzing and Formatting Protein and DNA Sequences. BioTechniques *28*, 1102–1104.
Strimmer, K., and von Haeseler, A. (1997). Likelihood-mapping: A simple method to visualize phylogenetic content of a sequence alignment. PNAS *94*, 6815–6819.
Sundberg, E., Slagter, J.G., Fridborg, I., Cleary, S.P., Robinson, C., and Coupland, G. (1997). ALBINO3, an Arabidopsis nuclear gene essential for chloroplast differentiation, encodes a chloroplast protein that shows homology to proteins present in bacterial membranes and yeast mitochondria. The Plant Cell *9*, 717–730.
Svensson-Ek, M., Abramson, J., Larsson, G., Törnroth, S., Brzezinski, P., and Iwata, S. (2002). The X-ray Crystal Structures of Wild-type and

EQ(I-286) Mutant Cytochrome c Oxidases from Rhodobacter sphaeroides. Journal of Molecular Biology *321*, 329–339.
Szyrach, G., Ott, M., Bonnefoy, N., Neupert, W., and Herrmann, J.M. (2003). Ribosome binding to the Oxa1 complex facilitates co-translational protein insertion in mitochondria. The EMBO Journal *22*, 6448–6457.
Tanaka, Y., Sugano, Y., Takemoto, M., Mori, T., Furukawa, A., Kusakizako, T., Kumazaki, K., Kashima, A., Ishitani, R., Sugita, Y., et al. (2015). Crystal Structures of SecYEG in Lipidic Cubic Phase Elucidate a Precise Resting and a Peptide-Bound State. Cell Reports *13*, 1561–1568.
The UniProt Consortium (2019). UniProt: a worldwide hub of protein knowledge. Nucleic Acids Research *47*, D506–D515.
Tipton, K. (2018). Translocases (EC 7): A new EC Class (International Union for Biochemistry and Molecular Biology).
Trifinopoulos, J., Nguyen, L.-T., von Haeseler, A., and Minh, B.Q. (2016). W-IQ-TREE: a fast online phylogenetic tool for maximum likelihood analysis. Nucleic Acids Research *44*, W232–W235.
Trifonov, E.N. (2000). Consensus temporal order of amino acids and evolution of the triplet code. Gene *261*, 139–151.
Van den Berg, B., Clemons Jr, W.M., Collinson, I., Modis, Y., Hartmann, E., Harrison, S.C., and Rapoport, T.A. (2004). X-ray structure of a protein-conducting channel. Nature *427*, 36.
Voorhees, R.M., and Hegde, R.S. (2016). Structure of the Sec61 channel opened by a signal sequence. Science *351*, 88–91.
Vothknecht, U.C., and Westhoff, P. (2001). Biogenesis and origin of thylakoid membranes. Biochimica et Biophysica Acta (BBA) - Molecular Cell Research *1541*, 91–101.
Wallin, E., and von Heijne, G. (1998). Genome-wide analysis of integral membrane proteins from eubacterial, archaean, and eukaryotic organisms. Protein Science *7*, 1029–1038.
Wang, F., Whynot, A., Tung, M., and Denic, V. (2011). The mechanism of tail-anchored protein insertion into the ER membrane. Molecular Cell *43*, 738–750.
Weber, A.L., and Miller, S.L. (1981). Reasons for the occurrence of the twenty coded protein amino acids. J Mol Evol *17*, 273–284.
Weiss, M.C., Sousa, F.L., Mrnjavac, N., Neukirchen, S., Roettger, M., Nelson-Sathi, S., and Martin, W.F. (2016). The physiology and habitat of the last universal common ancestor. Nature Microbiology *1*, 1–8.
Welte, T., Kudva, R., Kuhn, P., Sturm, L., Braig, D., Müller, M., Warscheid, B., Drepper, F., and Koch, H.-G. (2011). Promiscuous targeting of polytopic membrane proteins to SecYEG or YidC by the Escherichia coli signal recognition particle. MBoC *23*, 464–479.
Weng, T.-H., Steinchen, W., Beatrix, B., Berninghausen, O., Becker, T., Bange, G., Cheng, J., and Beckmann, R. (2020). Architecture of the active post-translational Sec translocon. EMBO J e105643.
White, S.H., and von Heijne, G. (2005). Transmembrane helices before, during, and after insertion. Curr Opin Struct Biol *15*, 378–386.
White, S.H., and Wimley, W.C. (1999). MEMBRANE PROTEIN FOLDING AND STABILITY: Physical Principles. Annual Review of Biophysics and Biomolecular Structure *28*, 319–365.
Wiedemann, N., and Pfanner, N. (2017). Mitochondrial Machineries for Protein Import and Assembly. Annual Review of Biochemistry *86*, 685–714.
Williams, T.A., Szöllősi, G.J., Spang, A., Foster, P.G., Heaps, S.E., Boussau, B., Ettema, T.J.G., and Embley, T.M. (2017). Integrative modeling of gene and genome evolution roots the archaeal tree of life. PNAS *114*, E4602–E4611.
Wu, X., Siggel, M., Ovchinnikov, S., Mi, W., Svetlov, V., Nudler, E., Liao, M., Hummer, G., and Rapoport, T.A. (2020). Structural basis of ER-associated protein degradation mediated by the Hrd1 ubiquitin ligase complex. Science *368*.
Xin, Y., Zhao, Y., Zheng, J., Zhou, H., Zhang, X.C., Tian, C., and Huang, Y. (2018). Structure of YidC from Thermotoga maritima and its implications for YidC-mediated membrane protein insertion. The FASEB Journal *32*, 2411–2421.
Xu, X., Ouyang, M., Lu, D., Zheng, C., and Zhang, L. (2020). Protein Sorting within Chloroplasts. Trends in Cell Biology.
Yang, J., Anishchenko, I., Park, H., Peng, Z., Ovchinnikov, S., and Baker, D. (2020). Improved protein structure prediction using predicted interresidue orientations. PNAS *117*, 1496–1503.
Yau, W.-M., Wimley, W.C., Gawrisch, K., and White, S.H. (1998). The Preference of Tryptophan for Membrane Interfaces. Biochemistry *37*, 14713–14718.
Yen, M.-R., Harley, K.T., Tseng, Y.-H., and Saier, M.H. (2001). Phylogenetic and structural analyses of the oxa1 family of protein translocases. FEMS Microbiol Lett *204*, 223–231.
Yi, L., Jiang, F., Chen, M., Cain, B., Bolhuis, A., and Dalbey, R.E. (2003). YidC Is Strictly Required for Membrane Insertion of Subunits a and c of the F1F0ATP Synthase and SecE of the SecYEG Translocase. Biochemistry *42*, 10537–10544.
Zeng, H., Wang, S., Zhou, T., Zhao, F., Li, X., Wu, Q., and Xu, J. (2018). ComplexContact: a web server for inter-protein contact prediction using deep learning. Nucleic Acids Res *46*, W432–W437.
Zhang, Y., Ou, X., Wang, X., Sun, D., Zhou, X., Wu, X., Li, Q., and Li, L. (2020). Structure of the mitochondrial TIM22 complex from yeast. Cell Research 1–3.
Zimmer, J., Nam, Y., and Rapoport, T.A. (2008). Structure of a complex of the ATPase SecA and the protein-translocation channel. Nature *455*, 936–943.
Zimmermann, L., Stephens, A., Nam, S.-Z., Rau, D., Kübler, J., Lozajic, M., Gabler, F., Söding, J., Lupas, A.N., and Alva, V. (2018). A Completely Reimplemented MPI Bioinformatics Toolkit with a New HHpred Server at its Core. Journal of Molecular Biology *430*, 2237–2243.

# Supplementary figures

**a** Structural similarity (TM-score)

| Taxon | State | C-half | N-half: 5aww | 3din | **6itc** | 7kb5 | **6fti** | 3jc2 | 1rh5 | mean |
|---|---|---|---|---|---|---|---|---|---|---|
| Bacteria | Closed | 5aww | 0.67 | 0.60 | 0.62 | 0.68 | 0.71 | 0.68 | 0.68 | 0.66 |
| | Primed | 3din | 0.65 | 0.64 | 0.62 | 0.65 | 0.62 | 0.65 | 0.67 | 0.64 |
| | Open | **6itc** | 0.74 | 0.69 | **0.75** | 0.77 | **0.81** | 0.77 | 0.77 | 0.76 |
| Eukarya | Closed | 7kb5 | 0.68 | 0.68 | 0.68 | 0.66 | 0.71 | 0.66 | 0.68 | 0.68 |
| | Primed | 6fti | 0.68 | 0.67 | 0.67 | 0.67 | 0.72 | 0.67 | 0.69 | 0.68 |
| | Open | 3jc2 | 0.69 | 0.68 | 0.68 | 0.68 | 0.72 | 0.70 | 0.70 | 0.69 |
| Archaea | Closed | 1rh5 | 0.67 | 0.64 | 0.64 | 0.65 | 0.70 | 0.65 | 0.66 | 0.66 |
| | | mean | 0.68 | 0.66 | 0.67 | 0.68 | 0.71 | 0.68 | 0.69 | |

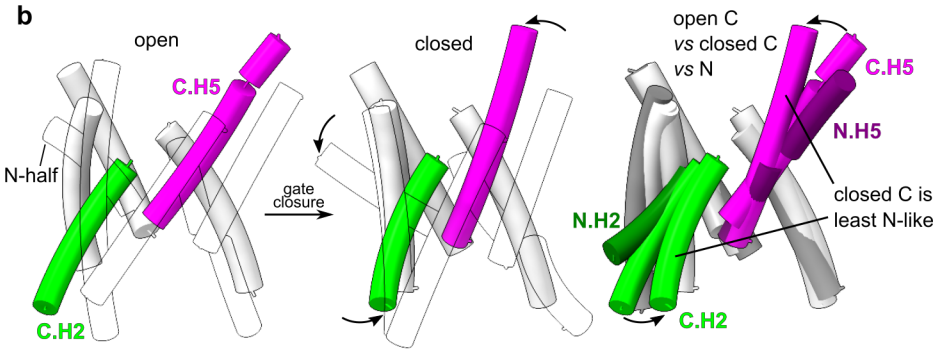


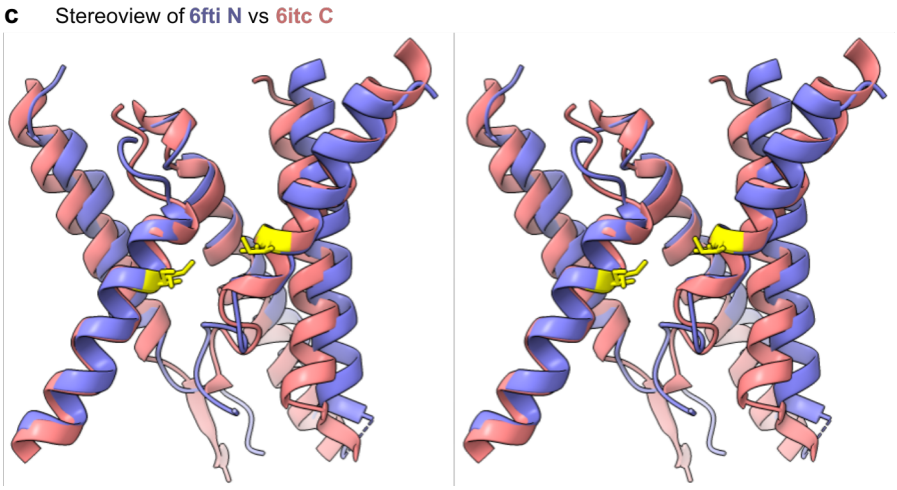


**Figure 2-Figure supplement 1.** Structural similarity and symmetry breaking between SecY halves. **a** Pairwise comparisons of the SecY halves by TM-score. TM-scores can range from 0 to 1. Boldface scores indicate the most similar pair from the same structure (6itc) or from any structure (6itc C, 6fti N). **b** Symmetry-breaking tilts in C.H2 and C.H5 induced by channel closure. At left, the TMHs from open (5aww) and closed (6itc) models are shown, with the N-half rendered in transparent outline. At right is a superposition of closed (5aww) and open C-halves (6itc) and an N-half (6itc). All models were aligned by H1/4. **c** Walleye stereoview of the most similar pair of N- and C-halves. The pore ring residues are shown as sticks and highlighted yellow.

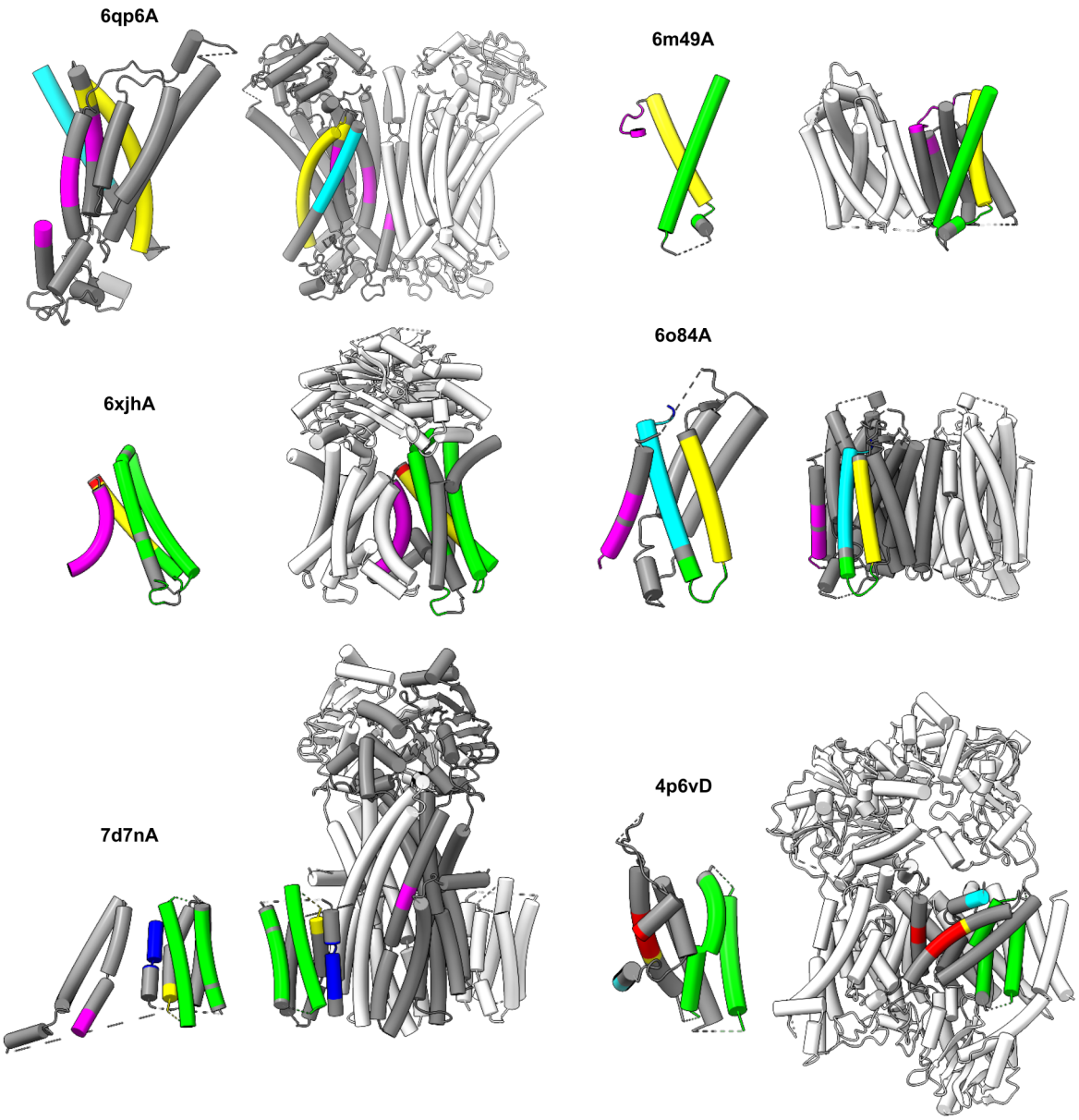


**Figure 3-Figure supplement 1.** Structures of non-Oxa1 superfamily top Dali hits. The aligned chain is shown in grey, and any other chains in the model are shown in white. Regions of each hit are colour-coded according to which part of the query structure they aligned with, using the colour scheme from Figure 4.

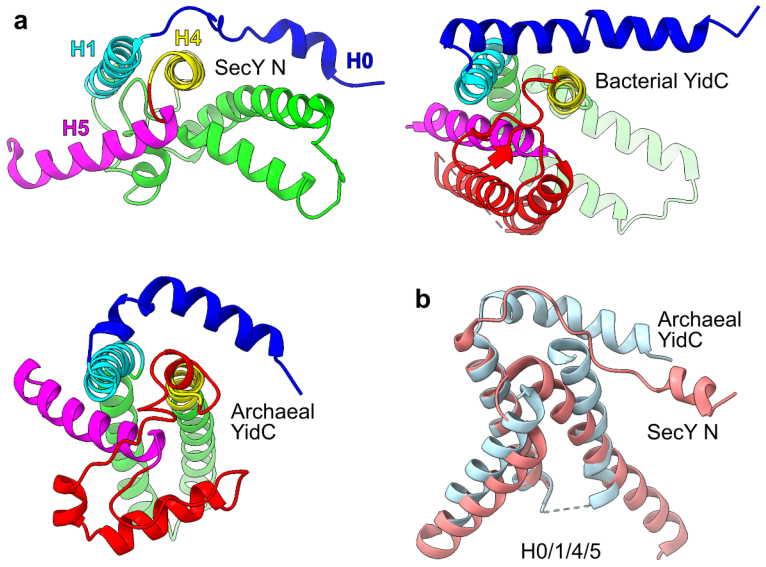


**Figure 4-Figure supplement 1.** Structural comparison of H0 in SecY and the Oxa1 superfamily. **a** Matched views of the SecY N-half (*M. jannaschii*, 1rhz), bacterial YidC (*B. halodurans* YidC2, 3wo6), and archaeal YidC (*M. jannaschii* MJ0480, see Figure 4-Figure supplement 4). **b** Alignment of YidC and SecY N, both from *M. jannaschii*.

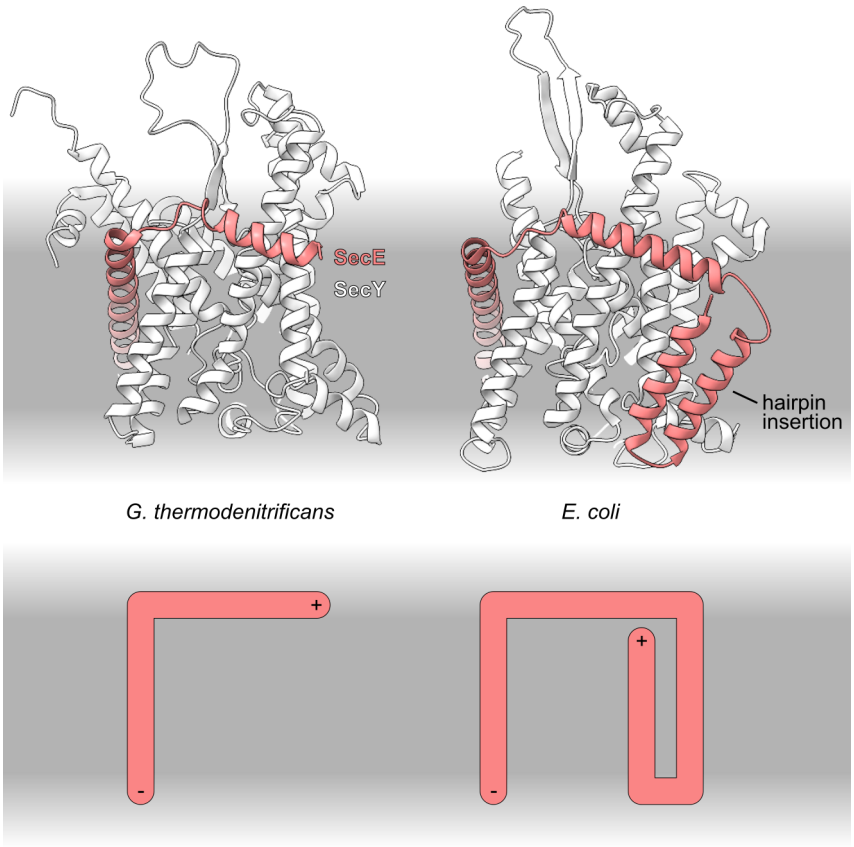


**Figure 4-Figure supplement 2.** Structure of the acquired transmembrane hairpin in SecE. Left: *G. thermodenitrificans* SecYE (6itc). Right: *E. coli* SecYE (6r7l; Kater et al., 2019). Top: molecular models of SecY (white) and SecE (light coral). Bottom: diagram of SecE topology, in which plus and minus signs indicate the N- and C-termini.

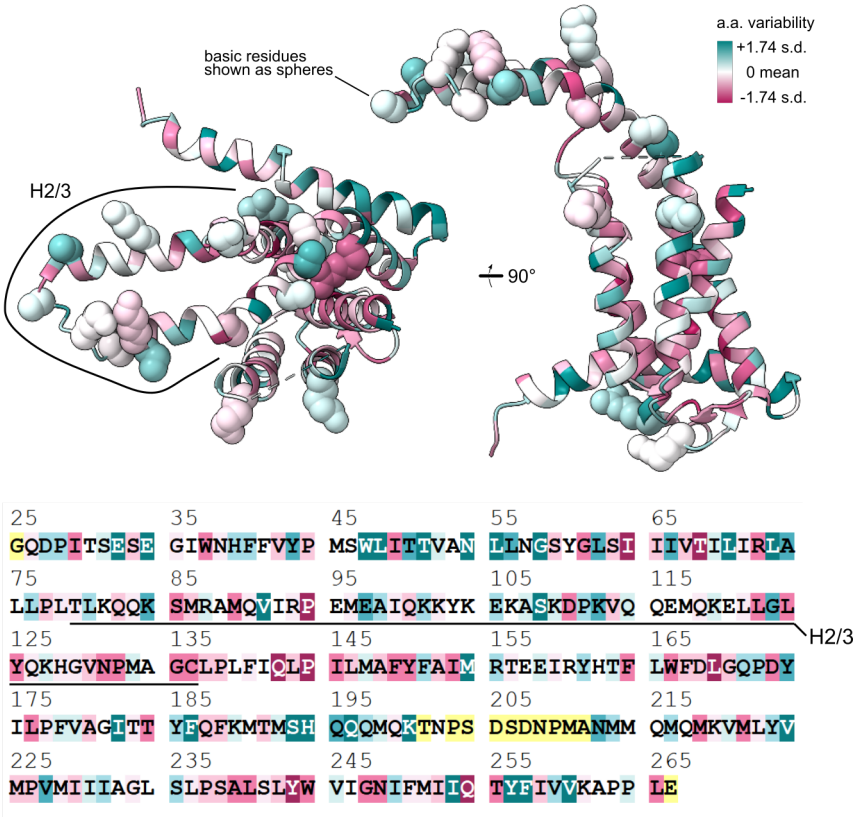


**Figure 4-Figure supplement 3.** Amino acid conservation in bacterial YidC. The conservation scores and annotated sequence and PDB model shown (*B. halodurans* YidC2, 3wo7A) were retrieved from ConSurf-DB (Chorin et al., 2020). The structure is colour-coded using the continuous scale shown, whereas the sequence is colour-coded on a similar but quantized scale. The scale shown encompasses the minimum but not maximum score.

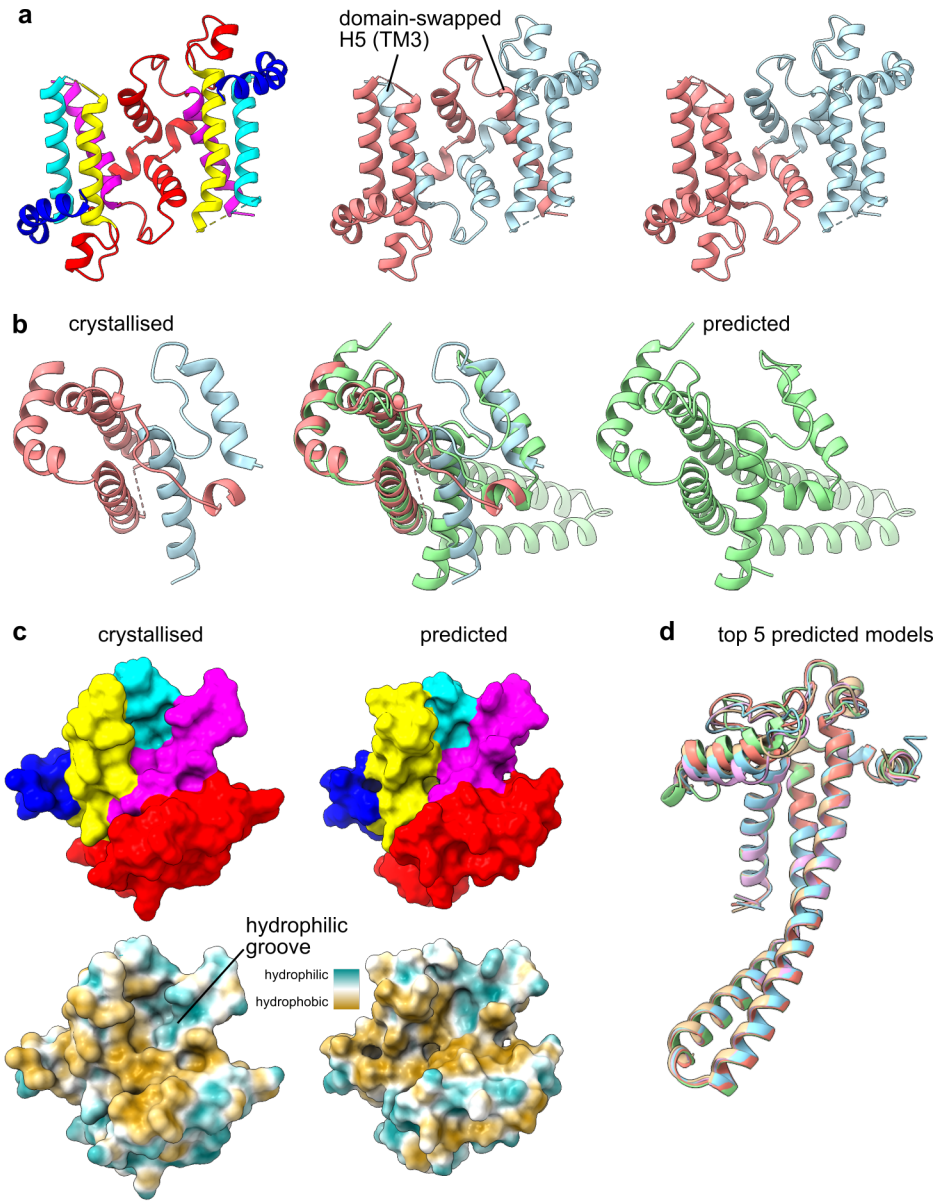


**Figure 4-Figure supplement 4.** Crystallised and predicted structures of archaeal YidC. **a** Domain swapping in crystallised archaeal YidC (*M. jannaschii* MJ0480 a.k.a. Ylp1, 5c8j). Left: colour-coded by consensus element as in Figure 4. Centre: colour-coded by chain. Right: colour-coded by chain, except the domain-swapped parts of H4/5 have been recoloured to match the chain against which it packs. **b** Alignment of the crystal structure (left, red and blue chains) with the trRosetta-predicted structure (right, green). **c** Comparison of the solvent-excluded surfaces of the crystallised and predicted structures, colour-coded by consensus element (top) or by hydropathy (bottom). **d** Alignment of the 5 highest-probability models built by trRosetta. The models were aligned by their first 40 amino acids.

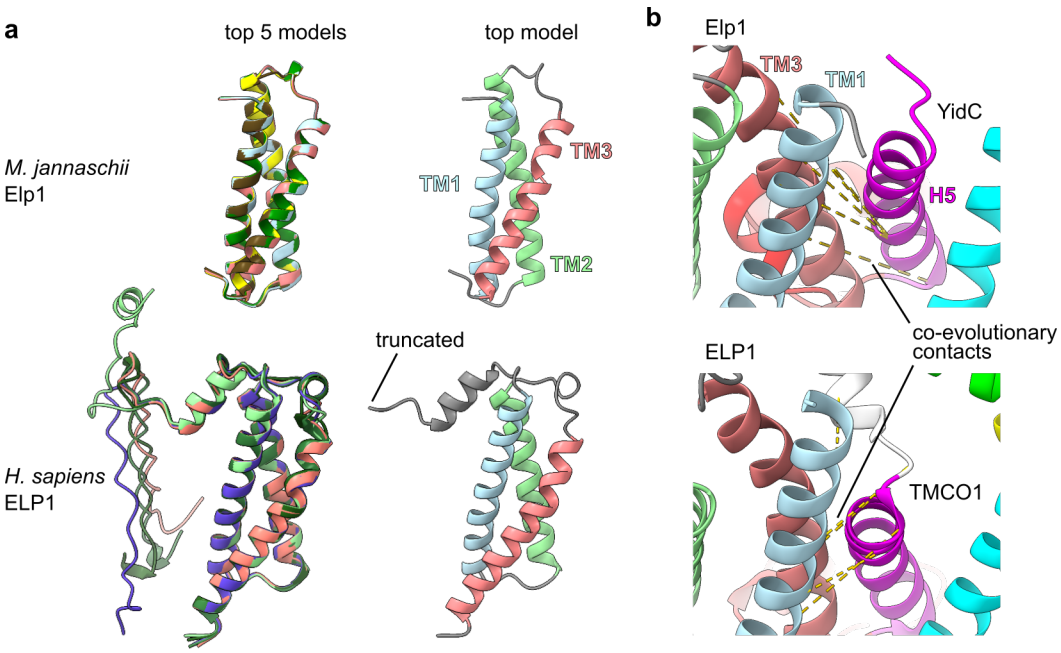


**Figure 8-Figure supplement 1.** Structure and contact prediction for archaeal and human EMC6-like proteins. **a** Alignment of the five highest-probability models determined by trRosetta (left) and an annotated view of the single best model (right), with disordered residues omitted. Models were predicted from the protein sequence of *M. jannaschii* Elp1 (MJ0606) and *H. sapiens* ELP1 (C20orf24). **b** Close-up view of the five highest-probability contacts between YidC/Elp1 and TMCO1/ELP1, represented by dashed gold lines.

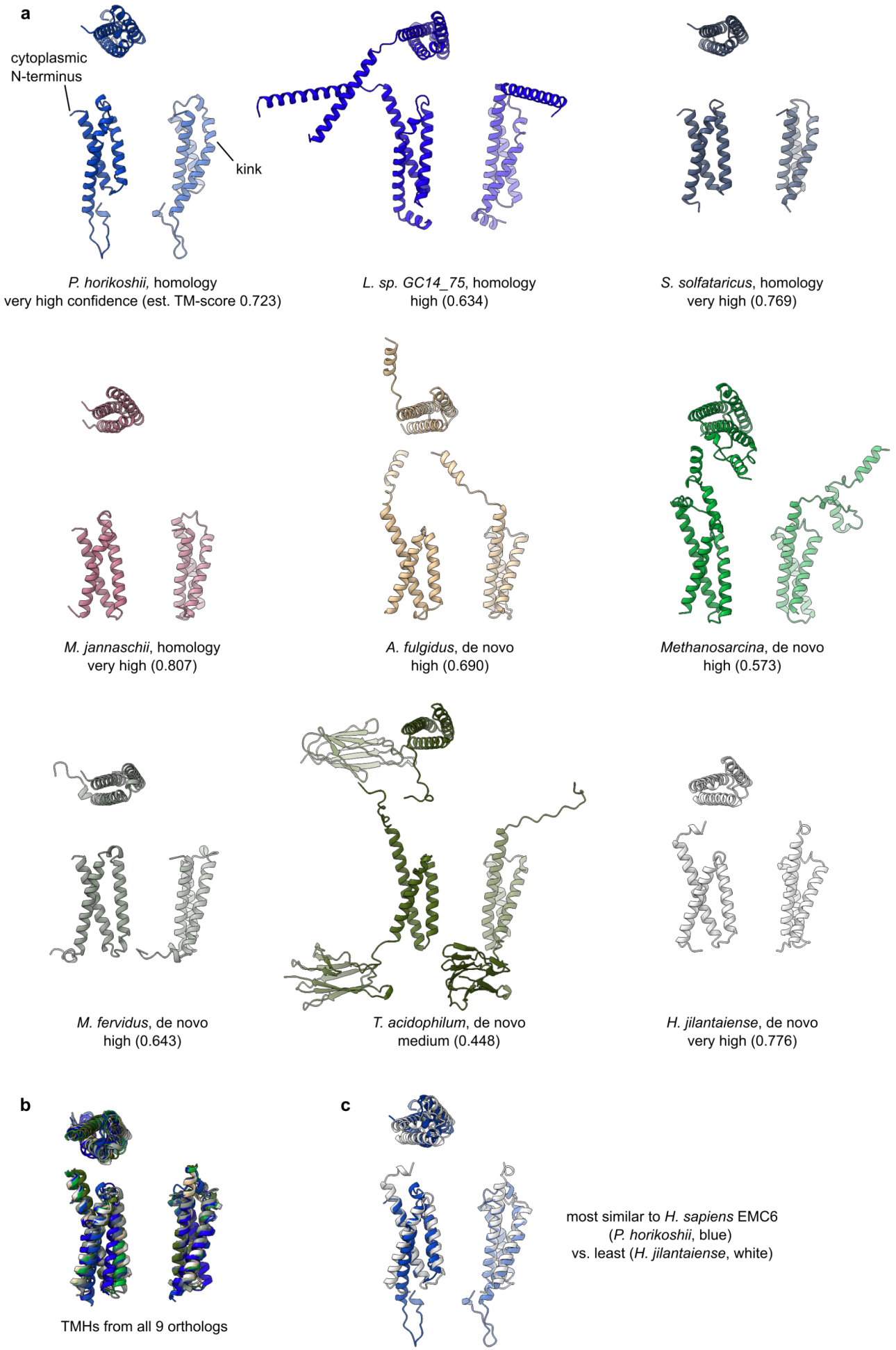


**Figure 8-Figure supplement 2.** Structural models for nine diverse archaeal EMC6-like proteins. **a** Front, top, and side views of each model, separated by 90° rotations. A kink in TM3 which is present in the homology models but absent from the *de novo* models is indicated. **b,c** Alignments of the indicated structural models.

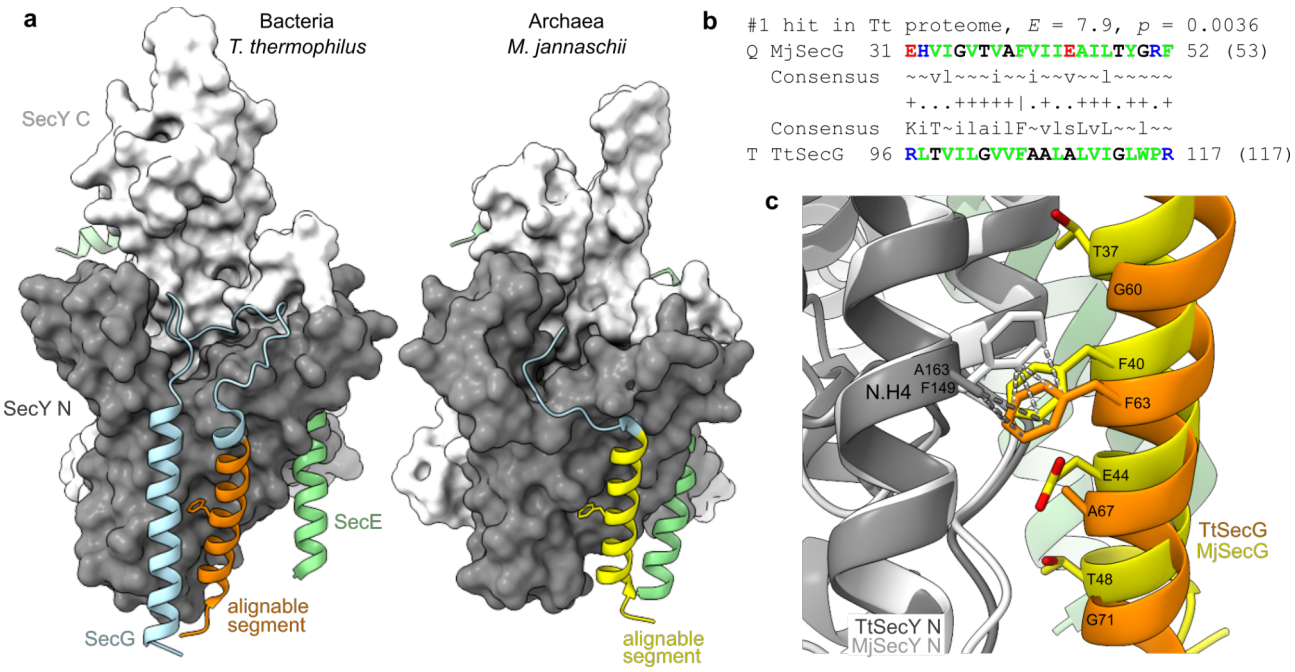


**Figure 11-Figure supplement 1.** Similarity between archaeal and bacterial SecG. **a** *T. thermophilus* and *M. jannaschii* SecYEG, shown separately but oriented by aligning the two SecY TMs against which SecG packs (N.H1 and N.H4). The SecG subsequences identified as homologous by HHpred (panel **b**) are highlighted in orange and yellow. **b** The top hit from an HHpred query of the *T. thermophilus* proteome with *M. jannaschii* SecG. **c** The hydrophilic face of SecG and a conserved phenylalanine which contacts a specific residue in SecY N.H4.